Redox Biology 55 (2022) 102400

Contents lists available at ScienceDirect

Redox Biology

journal homepage: www.elsevier.com/locate/redox

# Mitochondria-targeted anti-oxidant AntiOxCIN$_4$ improved liver steatosis in Western diet-fed mice by preventing lipid accumulation due to upregulation of fatty acid oxidation, quality control mechanism and antioxidant defense systems

Ricardo Amorim [a,b,c,1], Inês C.M. Simões [d,1], José Teixeira [a,1], Fernando Cagide [b,1], Yaiza Potes [d], Pedro Soares [b], Adriana Carvalho [a,c], Ludgero C. Tavares [a,e], Sofia Benfeito [b], Susana P. Pereira [a,g], Rui F. Simões [a,c], Agnieszka Karkucinska-Wieckowska [f], Ivan Viegas [h], Sylwia Szymanska [f], Michał Dąbrowski [d], Justyna Janikiewicz [d], Teresa Cunha-Oliveira [a], Agnieszka Dobrzyń [d], John G. Jones [a], Fernanda Borges [b,***,2], Mariusz R. Wieckowski [d,**,2], Paulo J. Oliveira [a,*,2]

[a] *CNC-Center for Neuroscience and Cell Biology, CIBB - Centre for Innovative Biomedicine and Biotechnology, University of Coimbra, 3004-504, Coimbra, Portugal*
[b] *CIQUP/Department of Chemistry and Biochemistry, Faculty of Sciences, University of Porto, Portugal*
[c] *PhD Programme in Experimental Biology and Biomedicine (PDBEB), Institute for Interdisciplinary Research (IIIUC), University of Coimbra, 3030-789, Coimbra, Portugal*
[d] *Laboratory of Mitochondrial Biology and Metabolism, Nencki Institute of Experimental Biology of Polish Academy of Sciences, Warsaw, Poland*
[e] *CIVG - Vasco da Gama Research Center, University School Vasco da Gama - EUVG, 3020-210, Coimbra, Portugal*
[f] *Department of Pathology, The Children's Memorial Health Institute, Warsaw, Poland*
[g] *Laboratory of Metabolism and Exercise (LametEx), Research Centre in Physical Activity, Health and Leisure (CIAFEL), Laboratory for Integrative and Translational Research in Population Health (ITR), Faculty of Sport, University of Porto, Porto, Portugal*
[h] *Centre for Functional Ecology, Department of Life Sciences, University of Coimbra, Coimbra, Portugal*

A B S T R A C T

Non-alcoholic fatty liver disease (NAFLD) is a health concern affecting 24% of the population worldwide. Although the pathophysiologic mechanisms underlying disease are not fully clarified, mitochondrial dysfunction and oxidative stress are key players in disease progression. Consequently, efforts to develop more efficient pharmacologic strategies targeting mitochondria for NAFLD prevention/treatment are underway. The conjugation of caffeic acid anti-oxidant moiety with an alkyl linker and a triphenylphosphonium cation ($TPP^+$), guided by structure-activity relationships, led to the development of a mitochondria-targeted anti-oxidant (AntiOxCIN$_4$) with remarkable anti-oxidant properties. Recently, we described that AntiOxCIN$_4$ improved mitochondrial function, upregulated anti-oxidant defense systems, and cellular quality control mechanisms (mitophagy/autophagy) via activation of the Nrf2/Keap1 pathway, preventing fatty acid-induced cell damage. Despite the data obtained, AntiOxCIN$_4$ effects on cellular and mitochondrial energy metabolism *in vivo* were not studied.

In the present work, we proposed that AntiOxCIN$_4$ (2.5 mg/day/animal) may prevent non-alcoholic fatty liver (NAFL) phenotype development in a C57BL/6J mice fed with 30% high-fat, 30% high-sucrose diet for 16 weeks. HepG2 cells treated with AntiOxCIN$_4$ (100 μM, 48 h) before the exposure to supraphysiologic free fatty acids (FFAs) (250 μM, 24 h) were used for complementary studies. AntiOxCIN$_4$ decreased body (by 43%), liver weight (by 39%), and plasma hepatocyte damage markers in WD-fed mice. Hepatic-related parameters associated with a reduction of fat liver accumulation (by 600%) and the remodeling of fatty acyl chain composition compared with the WD-fed group were improved. Data from human HepG2 cells confirmed that a reduction of lipid droplets size and number can be a result from AntiOxCIN$_4$-induced stimulation of fatty acid oxidation and mitochondrial OXPHOS remodeling. In WD-fed mice, AntiOxCIN$_4$ also induced a hepatic metabolism remodeling by upregulating mitochondrial OXPHOS, anti-oxidant defense system and phospholipid membrane composition, which is mediated by the PGC-1α-SIRT3 axis. AntiOxCIN$_4$ prevented lipid accumulation-driven autophagic flux impairment, by increasing lysosomal proteolytic capacity.

* Corresponding author. CNC - Center for Neuroscience and Cell Biology, CIBB – Center for Innovative Biomedicine and Biotechnology, University of Coimbra, Coimbra, Portugal.
** Corresponding author. Nencki Institute of Experimental Biology of Polish Academy of Sciences, Warsaw, Poland.
*** Corresponding author. CIQUP/Department of Chemistry and Biochemistry, Faculty of Sciences, University of Porto, Porto, Portugal.
*E-mail addresses:* fborges@fc.up.pt (F. Borges), m.wieckowski@nencki.edu.pl (M.R. Wieckowski), pauloliv@cnc.uc.pt (P.J. Oliveira).
[1] These authors contributed equally.
[2] These authors share senior authorship.

https://doi.org/10.1016/j.redox.2022.102400
Received 27 April 2022; Received in revised form 5 July 2022; Accepted 6 July 2022
Available online 16 July 2022

AntiOxCIN$_4$ improved NAFL phenotype of WD-fed mice, via three main mechanisms: a) increase mitochondrial function (fatty acid oxidation); b) stimulation anti-oxidant defense system (enzymatic and non-enzymatic) and; c) prevent the impairment in autophagy. Together, the findings support the potential use of AntiOxCIN$_4$ in the prevention/treatment of NAFLD.

**Abbreviations**

| | |
|---|---|
| ΔΨm | mitochondrial transmembrane electric potential |
| 4-HNE | 4-hydroxy-2-nonenal |
| AA | antimycin-A |
| ABTS | 2,2′-azino-bis(3-ethylbenzothiazoline-6-sulfonic acid) |
| AKT | protein kinase B complex |
| ALT | alanine aminotransferase |
| AMPK | AMP-activated protein kinase |
| AST | aspartate aminotransferase |
| BCA | bicinchoninic acid |
| BSA | bovine serum albumin |
| CAT | catalase |
| CE | cholesteryl esters |
| Chol | free cholesterol |
| DAG | diacylglycerols |
| DNL | *de novo* lipogenesis |
| DNP | dinitrophenol |
| DTNB | 5,5′-dithio-bis-(2-nitrobenzoic acid) |
| DTT | dithiothreitol |
| ER | endoplasmic reticulum |
| FAs | fatty acids |
| FAO | fatty acid oxidation |
| FCCP | carbonyl cyanide-4-(trifluoromethoxy)phenylhydrazone |
| FFAs | free fatty acids |
| G6PC | glucose-6-phosphatase |
| GAPDH | glyceraldehyde 3-phosphate dehydrogenase |
| GR | glutathione reductase |
| GSH | glutathione |
| H&E | hematoxylin & eosin |
| HFD | high-fat diet |
| LAMP2 | lysosome-associated membrane protein 2 |
| LC-MS/MS | liquid chromatography-mass spectrometry |
| LD | lipid droplets |
| MAS | mitochondrial assay solution |
| MDA | malondialdehyde |
| mPTP | mitochondrial permeability transition pore |
| MS | mass spectrometry |
| MTBE | methyl *tert*-butyl ether |
| mTOR | mammalian target of rapamycin complex |
| mtDNA | mitochondrial DNA |
| mtROS | mitochondrial ROS |
| NADPH | nicotinamide-adenine dinucleotide phosphate |
| NAFLD | non-alcoholic fatty liver disease |
| NAS | NAFLD score |
| NASH | non-alcoholic steatohepatitis |
| NMR | nuclear magnetic resonance |
| OCR | oxygen consumption rate |
| Olig | oligomycin |
| OxS | oxidative stress |
| PC | phosphatidylcholine |
| PCA | principal component analysis |
| PCK2 | phosphoenolpyruvate carboxykinase |
| PCX | pyruvate carboxylase |
| PE | phosphatidylethanolamine |
| PGK2 | phosphoglycerate kinase 2 |
| PHSF | primary human skin fibroblasts |
| PL | phospholipids |
| qPCR | quantitative polymerase chain reaction |
| ROS | reactive oxygen species |
| SD | standard diet |
| SDS-PAGE | sodium dodecyl-sulfate polyacrylamide gel electrophoresis |
| SFAs | saturated fatty acids |
| SIRT | sirtuin |
| SOD | superoxide dismutase |
| RCR | respiratory control ratio |
| tBHP | *tert*-butylhydroperoxide |
| TCA | tricarboxylic acid |
| TMPD | N,N,N′,N’-tetramethyl-p-phenylenediamine |
| TLC | thin layer chromatography |
| TNB | 2-nitro-5-thiobenzoate acid |
| TG | triglycerides |
| WD | western diet |

## 1. Introduction

Non-alcoholic fatty liver disease (NAFLD) has become a worldwide public health concern as metabolic syndrome-associated disorders rise. Although the cellular mechanisms behind NAFLD pathogenesis are still controversial, a redox imbalance promoted by exacerbated reactive oxygen species (ROS) is described to contribute to hepatotoxicity and proinflammatory processes [1]. These events ultimately trigger disease progression from early stage (non-alcoholic fatty liver (NAFL) into non-alcoholic steatohepatitis (NASH) and fibrosis. Accumulating evidence of oxidative stress (OxS)-related events in NAFLD stimulated the research to discover antioxidant-based therapies. For instance, vitamin E reduced serum alanine aminotransferase (ALT) levels and hepatic inflammation in NASH patients. However, no improvement in fibrosis was observed [2]. Similarly, silymarin did not reduce NAFLD activity score (NAS) in NASH patients, in phase II clinical trials [3].

Concomitantly, impairments in mitochondrial function have been extensively described to contribute to NAFLD progression spurring actively drug discovery focused on mitochondrial pharmacology [4]. MitoQ, the mitochondria-targeted golden standard anti-oxidant, decreased OxS, cell death and inflammation, reducing liver fibrosis in carbon tetrachloride ($CCl_4$)-treated C57BL/6J mice [5]. Nonetheless, MitoQ have failed or had minimal beneficial effects in clinical trials of OxS-related disorders, such as Parkinson’s disease or hepatitis C [6,7].

Moreover, autophagic pathway blockage contributes to exacerbate hepatocyte lipid accumulation and subsequent NAFLD worsening due to impaired regulation of lipophagy [8]. Several polyphenol anti-oxidants have been considered autophagic inducers [9,10]. Although caffeic acid improved hepatic steatosis in high-fat diet (HFD)-fed mice by stimulating autophagy [11], it was shown to have poor permeability across human colorectal Caco-2 cells, low intestinal absorption, and low oral bioavailability in rodents [12].

NAFLD is a complex and multifactorial disease, which is currently the focus of intense research. New potential drug candidates presenting target-specific affinity (mitochondria engagement) and the ability to regulate several cellular processes (mitochondrial redox status and

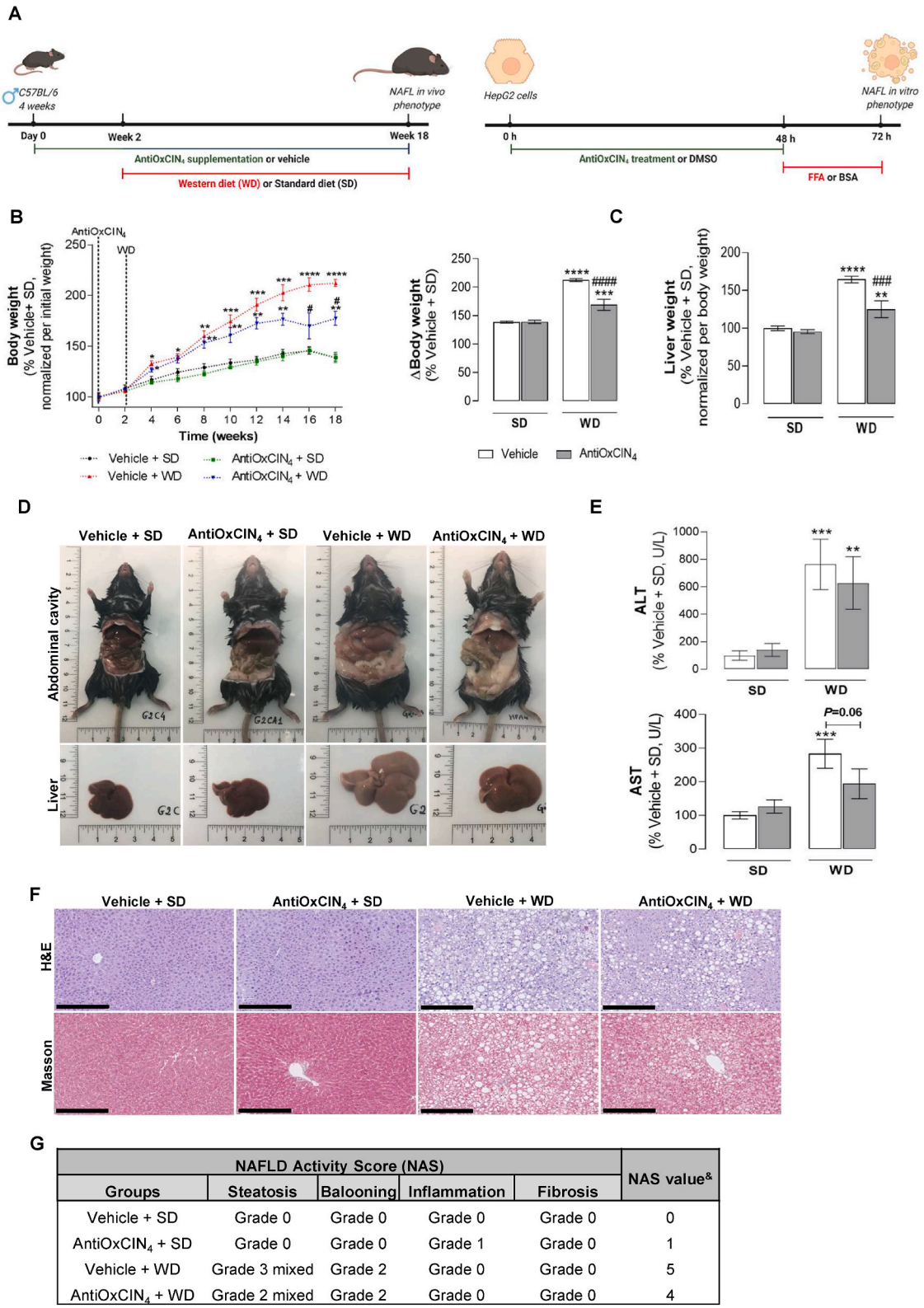


G

| NAFLD Activity Score (NAS) | | | | | NAS value[&] |
|---|---|---|---|---|---|
| Groups | Steatosis | Balooning | Inflammation | Fibrosis | |
| Vehicle + SD | Grade 0 | Grade 0 | Grade 0 | Grade 0 | 0 |
| AntiOxCIN$_4$ + SD | Grade 0 | Grade 0 | Grade 1 | Grade 0 | 1 |
| Vehicle + WD | Grade 3 mixed | Grade 2 | Grade 0 | Grade 0 | 5 |
| AntiOxCIN$_4$ + WD | Grade 2 mixed | Grade 2 | Grade 0 | Grade 0 | 4 |

**Fig. 1. Effects of AntiOxCIN$_4$ on body and liver weight, hepatocellular injury hallmarks and hepatic histology in a WD-fed mice with NAFL phenotype**. (A) Animal and human cells study experimental timelines. (B) Body weight progression along 18 weeks of anti-oxidant regimen and 16-weeks of diet (SD or WD) (left). Body weight from euthanized animals at 18$^{th}$ week of intervention (right). (C) Wet liver weight from euthanized animals. (D) Representative images of body and abdominal cavity (upper) and livers (lower) of euthanized mice. (E) Plasma AST and ALT activity levels in WD-fed mice in the absence/presence of AntiOxCIN$_4$ (2.5 mg/day/animal). (F) Representative histological images of liver sections stained with H&E and Masson's Trichrome stainings. Scale bar: 250 μm with 10x magnification. (G) NAFLD activity score (NAS) evaluation following guidelines provided in **SI**. [&]represents the sum of steatosis, hepatocyte ballooning, lobular inflammation and fibrosis grades obtained. Data are expressed as the mean ± SEM (N = 5 per cage) and the results were normalized to the respective control condition (set as 100%). Statistically significant compared using two-way ANOVA followed by Fisher's LSD test for multiple comparisons (*P < 0.05, **P < 0.01, ***P < 0.0005, ****P < 0.0001 vs Vehicle +SD); ($^{\#}$P < 0.05, $^{\#\#\#}$P < 0.0005,$^{\#\#\#\#}$P < 0.0001 vs Vehicle + WD).

autophagy) to confer protection against oxidative insults are needed. Previously, we demonstrated that a mitochondriotropic anti-oxidant based on caffeic acid (AntiOxCIN$_4$) prevented OxS-related events through activation of endogenous ROS-protective pathways in normal primary human fibroblasts (PHSF) [13] and in PHSF from sporadic Parkinson disease patients [14]. AntiOxCIN$_4$ also increased cell stress resistance in human hepatoma-derived cells (HepG2) by activating the Nrf2-p62-Keap1 axis, leading to up-regulation of anti-oxidant defenses, triggering macroautophagy and/or mitochondrial autophagy (mitophagy) and mitochondrial biogenesis. AntiOxCIN$_4$ switch on the mitochondrial metabolism, contributing to cell resistance to OxS and lipotoxicity events [15].

In this work, we identified the therapeutic benefits of AntiOxCIN$_4$ supplementation in a Western diet (WD)-induced NAFL mouse model. Mechanistic evidence in human hepatocytes (HepG2) subjected to supraphysiological FFA were acquired to supplement the *in vivo* data. Our study shows the potential mechanism of action for AntiOxCIN$_4$ supplementation improving steatotic liver phenotype in a NAFL mice model. The remarkable effects of AntiOxCIN$_4$ supplementation on fatty acid oxidation (FAO), endogenous anti-oxidant defense stimulation and prevention of autophagic blockage in WD-fed mice highlight AntiOxCIN$_4$ as a potential candidate for the prevention/treatment of NAFLD.

## 2. Materials and methods

**Chemicals and reagents.** Cell culture medium, medium components, chemicals and reagents were purchased from Sigma-Aldrich (St. Louis, MO, USA) unless otherwise specified.

**Synthesis and characterization of AntiOxCIN$_4$.** The synthetic strategy and procedures used in synthesizing the mitochondriotropic anti-oxidant AntiOxCIN$_4$ have been previously described [16]. The structural elucidation and stability data of AntiOxCIN$_4$ was evaluated by Nuclear Magnetic Resonance (NMR) and Mass (MS) Spectrometry. The $^1$H and $^{13}$C NMR spectra were acquired at room temperature and recorded on a Bruker Avance III operating at 400 and 100 MHz, respectively, while mass spectrum (MS) was recorded on a Bruker Microtof (ESI) or Varian 320-MS (EI) apparatus. HPLC analysis was performed on a Shimadzu Prominence HPLC SPD-M20A system (Shimadzu, Kyoto, Japan) to attest compound purity. Chromatograms were collected between 190 and 800 nm (Fig. S1A). The structural data is following the literature [16], while the purity of AntiOxCIN$_4$ was higher than 98%. Details are provided in Supporting Information (**SI**).

**Ethics.** The animal study was approved by the Animal Welfare Committee at the University of Coimbra (ORBEA_131_2016/24032016) and by the Portuguese Authority of Directorate-General for Food and Veterinary (DGAV - 0421/000/000/2016). All the procedures were also conducted following the European Union directive (2010/63/EU) by accredited users.

**Animal study.** Four-week-old male C57BL/6J mice were obtained from Charles River Laboratories France S.A.S. (Charles River, Barcelona, Spain). Animals were housed under controlled 12 h light/dark cycles at 20-24 °C with 45–65% of humidity. At the beginning of the study, animals (n = 20) were divided into 2 experimental groups: in the first one (n = 10), mice were fed with a standard chow diet (SD) and a vehicle sugar-free jelly (daily) (Vehicle +SD), whereas in the other group (n = 10), mice were fed with SD and a sugar-free jelly containing AntiOxCIN$_4$ (2.5 mg/animal/day) (AntiOxCIN$_4$ + SD). After 2 weeks, each experimental group was sub-divided into other two groups: half of the mice were maintained in SD while the other half of the mice were fed with a "Western diet" (WD) for 16 weeks (Fig. 1A). Details are provided in the **SI**. The group of mice fed with vehicle +SD was established as the control group of the study. After a total of 18 weeks feeding period, mice were anesthetized by isoflurane inhalation and animal euthanasia was performed by cervical dislocation.

**Plasma analysis.** Alanine aminotransferase (ALT) and aspartate aminotransferase (AST) activity levels, indicators of hepatocyte function, and cholesterol levels were measured using commercially available kits (A-R0200001001, A-R0200001101 and A-R0100000501, respectively; I.S.E. S.r.l., Guidonia, Italy) according to the manufacturer's protocol in an automated analyzer Miura 200 (I.S.E. S.r.l.).

**Liver histology.** For hematoxylin and eosin (H&E), Masson trichrome and immunohistological stainings, excised livers were fixed in 10% neutral buffered formalin (HT 50-1-1) for 48 h at room temperature. Then, the tissue was trimmed and processed for paraffin embedding (**see SI**).

**Isolation of liver mitochondria.** Isolation of hepatic mitochondrial fractions was performed by differential centrifugation as described in the **SI**.

**Evaluation of oxygen consumption rate (OCR) in isolated liver mitochondria.** The OCR of isolated hepatic mitochondria was measured at 37 °C using the Seahorse XFe96 Extracellular Flux Analyzer (Agilent Scientific Instruments, California, USA) as described in the **SI**.

**Evaluation of mitochondrial permeability transition pore (mPTP) opening in isolated liver mitochondria.** mPTP opening was measured by following mitochondrial swelling, estimated by alterations of light scattered from mitochondrial suspensions, as monitored spectrophotometrically at 540 nm using a Biotek Cytation 3 reader (Biotek Instruments, Winooski, VT, USA). The experiments were initiated by adding a suitable concentration of mPTP inducers: *tert*-butyl hydroperoxide (tBHP) and $CaCl_2$, titrated every day (**see SI**).

**Evaluation of $H_2O_2$ production in isolated liver mitochondria.** Mitochondrial $H_2O_2$ production was measured using Amplex Red Hydrogen Peroxide/Peroxidase Assay Kit (A22188, ThermoFisher Scientific) following manufacturer's instructions (**see SI**).

**Lipidomic analysis.** Liver lipids were extracted following the Bligh and Dyer method. Mitochondrial phospholipids were separated in a thin layer chromatography (TLC) tank using chloroform/methanol/acetic acid/water (50/37.5/3.5/2 (v/v/v/v)) as the mobile solvent for approximately 2 h, while neutral lipids were separated in a TLC tank using heptane/isopropyl ether/glacial acetic acid (60/40/3 (v/v/v)) as a mobile phase for 1 h.

Different mitochondrial phospholipids and neutral lipids bands were revealed by soaking the TLC plate in a 10% cupric sulfate/8% phosphoric acid and heated at 140 °C for 20 min and quantified with Image Studio Lite (version 5.2) (**see SI**).

**Metabolomic analysis.** Metabolomic analysis of hepatic triglycerides (TG) was obtained from $^1$H and $^{13}$C nuclear magnetic resonance (NMR) spectra (**see SI**).

**Total anti-oxidant capacity.** Anti-oxidant activity of cytosolic and mitochondrial fractions was measured by the capacity to decrease the amount of the 2,2′-azino-bis (3-ethylbenzothiazoline-6-sulfonic acid) (ABTS) radical monitored spectrophotometrically at 730 nm in a microplate reader (Infinite 200Pro, Tecan, Männedorf, Switzerland) for 15 min (**see SI**).

**Measurement of glutathione (GSH) levels.** GSH levels in the liver lysates were determined by monitoring the rate of 2-nitro-5-thiobenzoic acid formation in a Cytation 3 multi-mode microplate reader (BioTek Instruments, Inc.) at 412 nm (**see SI**).

**Measurement of catalase, superoxide dismutase (SOD) and glutathione reductase (GR) anti-oxidant activities.** Catalase activity was assessed in isolated mitochondria through the capacity to decompose $H_2O_2$ (**see SI**). Total SOD activity was determined in isolated mitochondria and liver lysates following the manufacturer's instructions (ADI-900-157, Enzo Life Sciences). GR activity was determined by following the reduction of GSSG to GSH as described in **SI**.

**Determination of aconitase activity.** Physiological and reactivated aconitase activity were assessed based on the protocols described in **SI**.

**Western blot analysis.** Protein content levels were analysed using sodium dodecyl-sulfate polyacrylamide gel electrophoresis (SDS-PAGE) of whole-liver homogenates or hepatic mitochondrial fractions from different mice groups. Then we perform Western blotting with antibodies against the denatured form of 4E-BP1 (sc9977, Santa Cruz

Biotechnology), AKT (#4691, Cell Signaling), LC3 (#12741, Cell Signaling,USA), mTOR (#2972, Cell Signaling), p-4E-BP1 (Thr45) (sc-271947, Santa Cruz Biotechnology), p62 (sc-28359, Santa Cruz Biotechnology), p-AMPKa (#2525, Cell Signaling), AMPKα (#5831, Cell Signaling), Beclin-1 (#3495, Cell Signaling) p-AKT (Ser473) (#4060, Cell Signaling), SIRT3 (#5490, Cell Signaling), PGC-1α (ST1202, Sigma-Aldrich) p-mTOR (#2971, Cell Signaling), p-p70S6K1 (Thr389) (#9205, Cell Signaling), p70S6K1 (sc-8418, Santa Cruz Biotechnology), Parkin (#4211, Cell Signaling), Pink1 (ab65232, Abcam), FIS1 (ab65232, Abcam), MFN2 (ab65232, Abcam), OPA-1 (ab65232, Abcam) and TOMM20 (ab65232, Abcam). The protein in liver lysates and cytosol was normalized by β-actin (A5441, Sigma-Aldrich) or glyceraldehyde 3-phosphate dehydrogenase (GAPDH) (#365062, Cell Signaling) while mitochondria protein was normalized by VDAC1 (ab34726, Abcam). The density of each band was calculated with T Image Studio Lite (version 5.2). Full details in **SI**.

**Proteomic analysis.** Liquid chromatography-mass spectrometry (LC-MS/MS) was performed at the Thermo Fisher Center for Multiplexed Proteomics (Department of Cell Biology, Harvard Medical School, Cambridge, MA, USA). Protein levels of whole liver homogenates from mice groups were visualized as heatmaps using Taverna Workbench Bioinformatics (version 2.5.0). Full details provided in SI, with the protein abbreviations represented in heatmaps detailed in SI Table 2.

**Measurement of cathepsin B activity.** Cathepsin B activity was measured by the cleavage of Z-Arg-Arg-N-methyl-coumarin (a fluorogenic substrate of cathepsin B) in whole liver homogenates of mice groups (**see SI**).

**Cell culture and AntiOxCIN$_4$ treatment.** Human hepatocellular carcinoma HepG2 cells (85011430, ECACC, UK) were cultured in low-glucose medium composed by Dulbecco's modified Eagle's medium (DMEM; D5030) supplemented with 5 mM glucose, sodium bicarbonate (3.7 g/L), HEPES (1.19 g/L), L-glutamine (0.876 g/L), sodium pyruvate (0.11 g/L), 10% fetal bovine serum (FBS), 1% penicillin-streptomycin 100x solution in a humidified atmosphere (5% $CO_2$, 37 °C). HepG2 cells were seeded (4.5 x $10^4$ cells/cm$^2$) and grown for 24 h until reaching 60–70% confluence. Then, cells were treated for 48 h with the mitochondriotropic anti-oxidant (AntiOxCIN$_4$, 100 μM) or vehicle (DMSO, 0.1%) following BSA (0.01 g/mL) or FFAs mixture (250 μM) treatment for 24 h period. Cell condition defined as Vehicle + BSA was established as the control group of the study.

**Free fatty acids (FFAs) conjugation.** FFAs mixtures were prepared as saponified 10 mM stock solutions and complexed (1:1) with free-fatty acids:BSA (10 min at 50 °C), cooled to room temperature. The free-fatty acids:BSA (0.2 g/mL) was diluted in the same proportion with 25 mM KOH. Details are provided as **SI**.

**Cell mass measurements.** Sulforhodamine B (SRB) assay was used for HepG2 cell mass determination (**see SI**).

**Mitochondrial membrane potential (ΔΨm) measurements.** HepG2 were stained with MitoTracker Red$^{FM}$ (100 nM; M22425, ThermoFisher Scientific) and Hoechst 33342 (1 μg/mL; H1399, ThermoFisher Scientific) for analysis of ΔΨm and quantification of mitochondrial morphology parameters using confocal fluorescent microscopy (**see SI**).

**Cellular oxidative stress detection.** Oxidative stress was assessed in living HepG2 by measuring the oxidation of CM-$H_2$-DCFDA redox indicator (C6827, ThermoFisher Scientific) (**see SI**).

**Evaluation of cellular fatty acids oxidation (FAO)-linked OCR.** FAO-linked OCR of HepG2 cells was measured at 37 °C using the Seahorse XFe96 Extracellular Flux Analyzer (Agilent Scientific Instruments) as described in the **SI**.

**Evaluation of neutral lipid content.** Neutral lipid accumulation in HepG2 cells was evaluated through the Nile Red-staining fluorescence at 636 nm as described in **SI**.

**Lipid Droplet (LD) Staining.** HepG2 were stained with LipidTOX™ Green (1:1000; H34475, ThermoFisher Scientific) and Hoechst 33342 (1 μg/mL; H1399, ThermoFisher Scientific) for analysis of LD and quantification of LD parameters using confocal fluorescent microscopy (**see SI**).

**Gene expression measurements.** Transcript analysis was assessed through quantitative polymerase chain reaction (qPCR) (see **SI**). Genes names are detailed in SI Table 3.

**Principal component analysis (PCA).** Details are provided in SI, with physiological mice features detailed in SI Table 4.

**Statistics.** Data were expressed as the mean value ± standard error of the mean (SEM). Statistical analysis was performed using GraphPad Prism version 8.0.2 (GraphPad Software Inc., San Diego, CA, USA). The normality of the data was assessed using the Shapiro-Wilk test. Non-normality data was analysed using the non-parametric Kruskal-Wallis test while with normal data was used the parametric test two-way ANOVA, followed by Fisher's LSD test for multiple comparisons. The level of significance considered was $^{*}P < 0.05$, $^{**}P < 0.01$, $^{***}P < 0.001$, $^{****}P < 0.0001$ for multiple comparisons vs SD or Vehicle + BSA and $^{\#}P < 0.05$, $^{\#\#}P < 0.01$, $^{\#\#\#}P < 0.0005$, $^{\#\#\#\#}P < 0.0001$ vs WD or Vehicle + FFAs.

## 3. Results

In this study, we evaluated the therapeutic benefits of a mitochondria-targeted phenolic acid anti-oxidant (AntiOxCIN$_4$) (Fig. S1A) supplementation in a Western diet (WD)-induced NAFL mice model, together with cellular and molecular *in vitro* data using human hepatocytes (HepG2) subjected to supraphysiological FFA. HPLC analysis demonstrated that the purity of AntiOxCIN$_4$ was higher than 98% (Fig. S1B), while the compound was stable in water for 3 h at room temperature (RT) (Fig. S1C). Additional NMR experiments, also confirmed AntiOxCIN$_4$ stability in DMSO over 24 h, as no signs of compound degradation at room temperature were observed (Fig. S1D).

**AntiOxCIN$_4$ decreased body weight and improved hepatic-related physiological parameters in a WD-fed mice model with a NAFL phenotype**. In this study, a rodent diet mimicking WD eating habits induced an increase in body weight (174%) along a sixteen-week feeding period compared to the Vehicle + SD mice group (Fig. 1B). AntiOxCIN$_4$ supplementation prevented WD-induced weight gain (Fig. 1B), being this effect significant from the 15$^{th}$ week of WD feeding until the time of euthanasia (by 43%). AntiOxCIN$_4$ did not interfere with weight gain in the animals fed with a standard diet. Upon AntiOxCIN$_4$ supplementation, no alterations were observed in food intake, water consumption (Fig. S2B), or animal welfare. Final body and liver weight were collected at euthanasia, as shown in Fig. S2A. Noteworthy, WD feeding also induced an increase of liver weight gain (164%) and size, which was significantly prevented by AntiOxCIN$_4$ supplementation (by 39%) (Fig. 1C and D). Plasma from WD-fed mice presented alterations in hepatocyte damage hallmarks such as increased aspartate aminotransferase (AST) (282%), alanine aminotransferase (ALT) (763%) activities (Fig. 1E), and cholesterol (Chol) (176%) levels (Fig. S2C). AntiOxCIN$_4$ decreased WD-induced increase of plasma ALT (by 134%), AST (by 89%) and cholesterol (by 18%) circulating levels when compared with the WD-fed mice (Figs. 1E and S2C).

Histological staining with H&E and Masson's trichrome revealed that the physiological outcomes of WD feeding are associated with the development of simple steatosis (NAFL) (Fig. 1F and G). The NAFL stage was characterized by mixed steatosis (grade 3), hepatocyte ballooning (grade 2), and the absence of inflammation and fibrosis (Fig. 1G, S2D and S2E), with a NAFLD Activity Score (NAS) of 5. AntiOxCIN$_4$ supplementation significantly diminished hepatic lipid accumulation, as shown by the reduction of the steatotic grade from 3 to 2 (Fig. 1F and G), which was translated into a decrease in NAS value. No alterations were observed at hepatocyte ballooning level compared with the Vehicle + WD group (Fig. 1F and G).

**AntiOxCIN$_4$ improved alterations in hepatic lipid profile in the liver of a WD-fed mice model with a NAFL phenotype.** Quantification of LD relative intensity in the H&E staining confirmed that Vehicle +

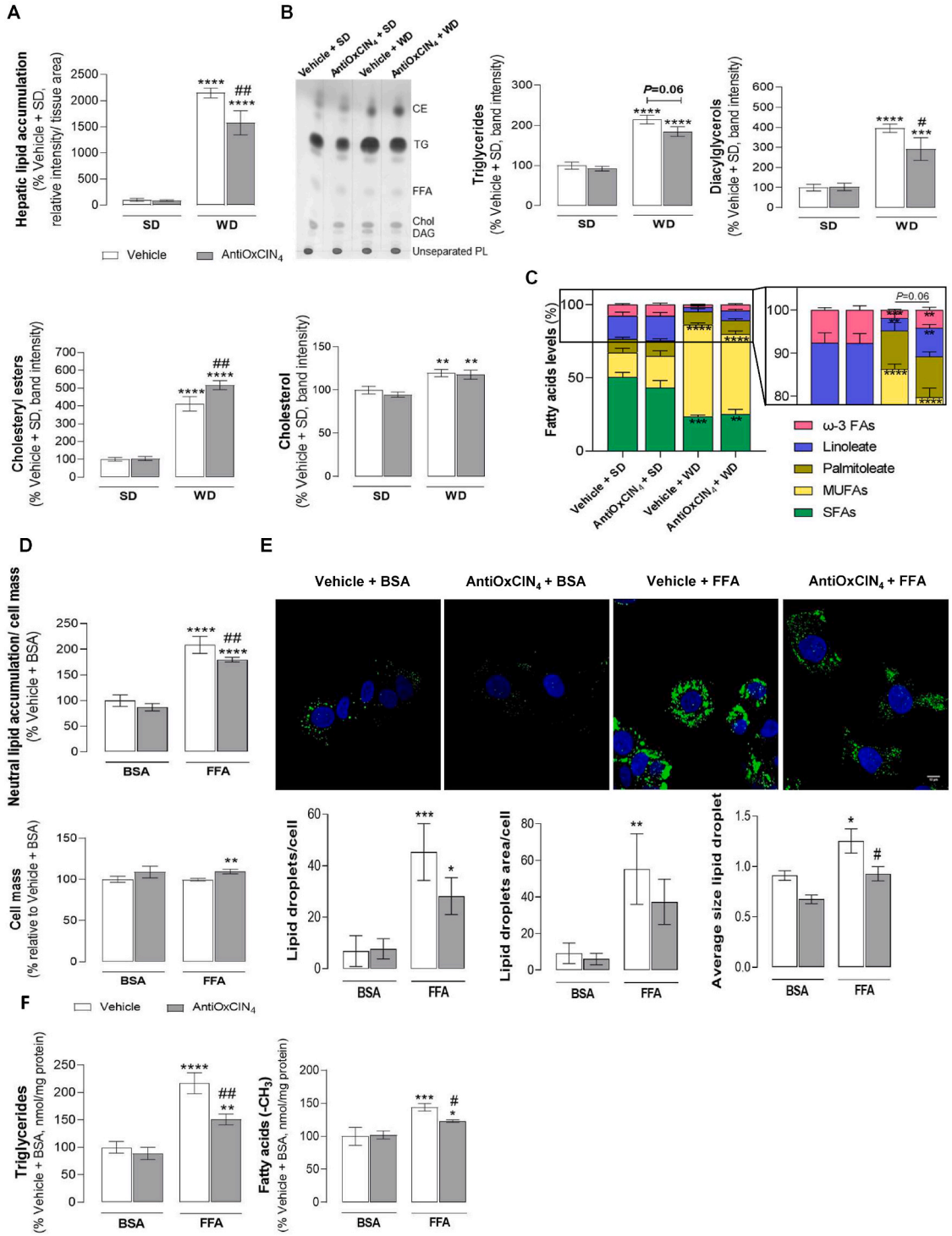


**Fig. 2. Effects of AntiOxCIN$_4$ on hepatic lipid content and composition of WD-fed mice and FFAs-treated human HepG2 cells.** (A) Hepatic lipid accumulation. Lipid quantification was obtained from three independent images/per animal of each experimental group of H&E staining. (B) Representative image of hepatic neutral lipid profile in WD-fed mice in the absence/presence of AntiOxCIN$_4$ (2.5 mg/day/animal) using thin-layer chromatography (TLC). Several parameters were evaluated: triglycerides (TGs), diacylglycerols (DAGs), cholesteryl esters (CEs) and free cholesterol (chol). (C) Fatty acyl chain composition of hepatic triglycerides in terms of saturated fatty acids, palmitoleate, oleate, linoleate and ω-3 fatty acids in liver homogenates from WD-fed mice in the absence/presence of AntiOxCIN$_4$ (2.5 mg/day/animal). (D) Neutral lipid accumulation (upper) and respective cell mass (lower) in human HepG2 cells treated with vehicle (BSA) or FFAs (24 h, 250 μM) in the absence/presence of AntiOxCIN$_4$ (48 h, 100 μM). (E) Typical background-corrected images of HepG2 cells stained with the LipidTOX Green (lipids, green) and Hoechst 33342 (nucleus, blue), and treated with vehicle (BSA) or FFAs (24 h, 250 μM) in the absence/presence of AntiOxCIN$_4$ (48 h, 100 μM) (upper). The LipidTOX Green and Hoechst 33342 fluorescence intensity was color-coded to green and blue, respectively. Average lipid droplet number, area and size was calculated from four images in multiple experiments (lower). (F) Triglycerides (left) and intracellular fatty acids (right) in cells treated with vehicle (BSA) or FFAs (24 h, 250 μM) in the absence/presence of AntiOxCIN$_4$ (48 h, 100 μM). Data are expressed as the mean ± SEM (N = 5 per cage for the *in vivo* study and N = 4 for the HepG2 studies) and the results were normalized to the respective control condition (set as 100%). Statistically significant compared using two-way ANOVA followed by Fisher's LSD test for multiple comparisons (*P < 0.05, **P < 0.01, ***P < 0.0005, ****P < 0.0001 vs SD or Vehicle + BSA); ($^{\#}$P < 0.05, $^{\#\#}$P < 0.01 vs WD or Vehicle + FFAs).

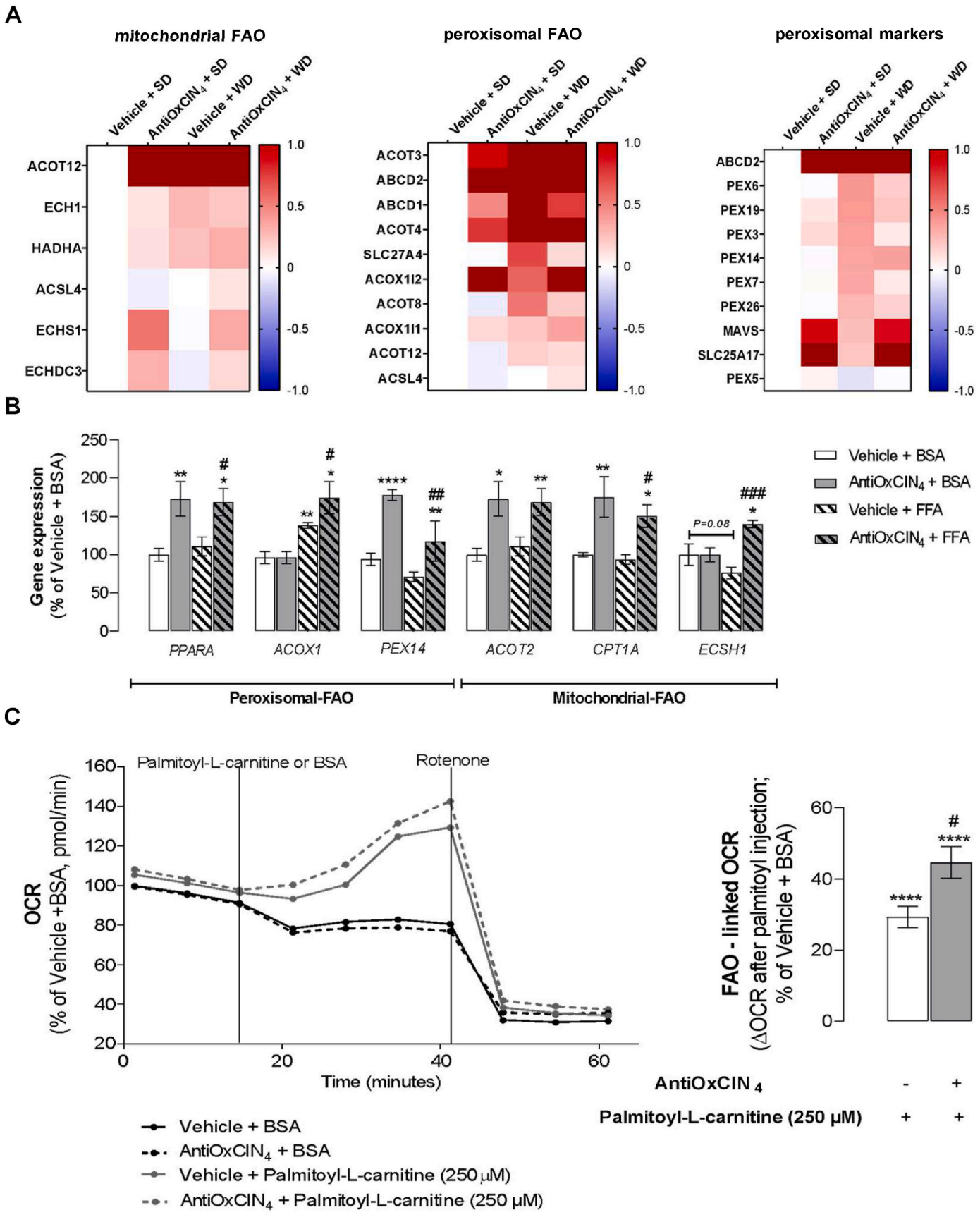


*(caption on next page)*

**Fig. 3. Effects of AntiOxCIN$_4$ on mitochondrial and peroxisomal fatty acid oxidation (FAO) of WD-fed mice and FFAs-treated human HepG2 cells.** (A) Mass spectrometry (MS)-proteomic analysis of hepatic mitochondrial, peroxisomal FAO-related proteins, and peroxisomal markers levels in WD-fed mice in the absence/presence of AntiOxCIN$_4$ (2.5 mg/day/animal). Blue color represents a decrease, while red color represents an increase of the protein levels. (B) mRNA transcript levels of FAO-related genes (*PPARα, ACOX1, PEX14, ACOT2, CPT1α,* and *ECSH1)* in human HepG2 cells treated with vehicle (BSA) or FFAs (24 h, 250 μM) in the absence/presence of AntiOxCIN$_4$ (48 h, 100 μM). (C) Representative image of FAO-related oxygen consumption rate (OCR) measurement. BSA or palmitoyl-L-carnitine (250 μM) were acutely injected in HepG2 in the absence/presence of AntiOxCIN$_4$ (48 h, 100 μM). Data are expressed as the mean ± SEM (N = 5 per cage for the *in vivo* study and N = 4 for the HepG2 studies) and the results were normalized to the control condition (set as 100%). Statistically significant compared using two-way ANOVA followed by Fisher's LSD test for multiple comparisons (*P < 0.05, **P < 0.01, ****P < 0.0001 vs SD or Vehicle + BSA); ($^{\#}$P < 0.05, $^{\#\#}$P < 0.01, $^{\#\#\#\#}$P < 0.0001 vs WD or Vehicle + FFAs).

WD increased hepatic lipid accumulation (2147%) when compared to the Vehicle + SD group (Fig. 2A). These observations are in agreement with MS-proteomic data by evidencing an increase of *de novo* lipogenesis (DNL) and elongation/unsaturation-related proteins in the Vehicle + WD group (Fig. S2E). The data from TLC analysis showed that hepatic tissue from WD-fed mice have increased TG (214%) and cholesteryl esters (CEs) (411%) content, with a concomitant increase of diacylglycerols (DAGs) (395%) and free Chol (119%) levels (Fig. 2B). WD feeding induced a decrease of saturated fatty acids (SFAs) levels (23%) in comparison with the Vehicle + SD group (50%) (Fig. 2C). Moreover, WD feeding favoured an enrichment of oleate (63%), while a decrease of linoleate (3%) and ω-3 FAs (2%) was noticed in comparison with oleate (17%), linoleate (15%) and ω-3 FAs (7%) of Vehicle +SD group (Fig. 2C). AntiOxCIN$_4$ *per se* did not alter the hepatic lipid profile of SD-fed mice (Fig. 2A–C). However, AntiOxCIN$_4$ supplementation induced the expression of proteins involved in DNL and in elongation/unsaturation-related pathways (Fig. S2F). In WD-fed mice, AntiOxCIN$_4$ supplementation decreased hepatic LD relative intensity (by 570%) when compared with Vehicle + WD group (Fig. 2A). Moreover, AntiOxCIN$_4$ also improved the lipid composition profile with a decrease in the TG (by 30%) and DAGs (by 103%) levels (Fig. 2B). Interestingly, AntiOxCIN$_4$ supplementation in WD-fed mice led to higher CEs levels (by 105%) while no significant differences were found in Chol levels (Fig. 2B). The data suggested that AntiOxCIN$_4$, in the presence of WD diet habits, can modulate FAs acyl chain composition, as demonstrated by a trending decrease in oleate (by 9%) and a non-statistically significant increase of linoleate (by 4%) and ω-3 FAs (by 2%) (Fig. 2C). Next, we performed principal component analysis (PCA) using the subset of physiological parameters described in SI Table 3. The measured parameters allow to discriminate the different experimental groups. Samples belonging to Vehicle + SD and AntiOxCIN$_4$ + SD cluster close to each other while Vehicle + WD sit distant from SD groups. Remarkably, AntiOxCIN$_4$ + WD cluster closer to SD groups (Fig. S2G). AntiOxCIN$_4$ improved hepatic lipid profile, indicating a healthier liver phenotype in NAFL models.

**AntiOxCIN$_4$ decreased LD size of FFAs-treated human HepG2 cells.** Cellular and molecular evidences in human hepatocytes (HepG2) were acquired to complement the *in vivo* data. AntiOxCIN$_4$ (48 h, 100 μM) counteracted the lipotoxicity of supraphysiological FFA concentrations (24 h, 250 μM). Control (BSA-treated) cells incubated with FFAs showed an increase in neutral lipid content (210%) without no signs of cell death (Fig. 2D). AntiOxCIN$_4$ incubation (48 h, 100 μM) before FFAs exposure significantly reduced lipid accumulation (by 29%) (Fig. 2D). Additionally, AntiOxCIN$_4$ pre-treatment showed to significantly reduced LD size while slightly decreased their abundance when compared with vehicle + FFA cells (Fig. 2E). Nuclear magnetic resonance (NMR) experiments also corroborated that AntiOxCIN$_4$ decreased TG and FAs levels in HepG2 cells exposed to FFAs (Fig. 2F).

**AntiOxCIN$_4$ increased mitochondrial and peroxisomal fatty acid oxidation (FAO) markers in the liver of WD-fed mice with a NAFL phenotype**. We next evaluated the effects of AntiOxCIN$_4$ in FAO, a key pathway responsible for FAs metabolism in hepatocytes under nutrient overload [17], in WD-fed mice. MS-proteomic analysis revealed that AntiOxCIN$_4$ + SD mice presented higher levels of mitochondrial-FAO related proteins (ACOT12, ECHS1 and ECHDC3), peroxisomal-FAO related proteins (ACOT3/4, ABCD1/2 transporters and ACOX1i2), and peroxisomal markers (SLC25A17 and MAVS) (Fig. 3A). Although WD feeding can also cause an increase in some of these FAO- and peroxisomal-related proteins, the AntiOxCIN$_4$ supplementation had a major impact in mitochondrial- and peroxisomal FAO-related enzymes and peroxisomal-related protein levels (Fig. 3A).

**AntiOxCIN$_4$ increased mitochondrial and peroxisomal fatty acid oxidation (FAO) markers and FAO-linked oxygen consumption in FFAs-treated human HepG2 cells**. The effect of AntiOxCIN$_4$ in both mitochondrial and peroxisomal FAO was also evaluated in human hepatoma cells (HepG2). In fact, AntiOxCIN$_4$ increased mRNA levels of peroxisome proliferator-activated receptor-*α* (*PPARA*) in both Vehicle + FFAs (169%) and in Vehicle + BSA (173%) regimens (Fig. 3B). PPAR*α* is a master regulator of FAO-related pathways, being its levels correlated with elevated mitochondrial-FAO (*ACOT2,* 169%; *CPT1A,* 151%, *ECHS1,* 140%) and peroxisomal-FAO related genes (*PEX14*, 117%; *ACOX1*, 174%) in AntiOxCIN$_4$ + FFAs condition. The markers *CPT1A* (175%), *ACOT2* (173%) and *PEX14* (178%) were also elevated in the BSA + AntiOxCIN$_4$ group (Fig. 3B). The functional cellular oxygen consumption rate (OCR) resulting from palmitoyl-L-carnitine oxidation was analysed to estimate the mitochondrial contribution for FAO. No significant differences were found between Vehicle + BSA and AntiOxCIN$_4$ + BSA-treated cells (Fig. 3C). Acute cell treatment with palmitoyl-L-carnitine led to an increase of 33% in FAO-linked OCR, being this parameter increased by 15% in AntiOxCIN$_4$ + palmitoyl-L-carnitine cells (Fig. 3C).

**AntiOxCIN$_4$ increased OXPHOS-coupled efficiency and prevented alterations in the mitochondrial phospholipid profile, decreasing the susceptibility to mitochondrial permeability transition pore (mPTP) opening in the liver of WD-fed mice with NAFL phenotype**. We next investigated whether AntiOxCIN$_4$ also impacts hepatic mitochondrial function of WD-fed mice. Liver mitochondrial fractions isolated from Vehicle + WD energized with pyruvate/malate showed an increase in ADP-stimulated respiration (st3) and maximal uncoupled respiration (st3u) OCR (Fig. 4A). AntiOxCIN$_4$ supplementation significantly prevented the WD-induced increase in st3u OCR (Fig. 4A). Moreover, AntiOxCIN$_4$ promoted a decrease in st3u in SD-fed mice (Fig. 4A). The respiratory control ratio (RCR, state 3/state 4°), a measure of OXPHOS-coupling efficiency, was decreased in liver mitochondria from Vehicle + WD group. This effect was partially prevented in AntiOxCIN$_4$ + WD group (Fig. 4B). Although similar results were observed for succinate-energized mitochondria (Fig. S3A), RCR remained unaltered in complex II-driven respiration (Fig. S3B) when compared with Vehicle +SD group. Notwithstanding, the analysis of mitochondrial electron transport chain activity (Fig. S3C) showed that WD feeding significantly increased mitochondrial complex I, II and IV activities, when compared with Vehicle +SD mice, although no differences were observed between both WD-fed groups (Vehicle + WD vs. AntiOxCIN$_4$ + WD) (Fig. S3D). Interestingly, mitochondrial complex II/IV activity ratio, an indicator of TCA cycle truncation [18], is only significantly increased in Vehicle + WD compared to Vehicle +SD mice (Fig. 4C). Next, we evaluated the susceptibility of the hepatic mitochondria to mPTP opening in the presence of $Ca^{2+}$ and *t*BHP. Isolated mitochondria from Vehicle + WD mice showed higher vulnerability to mPTP opening (150%), an effect that was (non-statistically) reduced by AntiOxCIN$_4$ supplementation (by 18%) (Fig. 4D). The analysis of mitochondrial phospholipid composition in the livers of steatotic mice

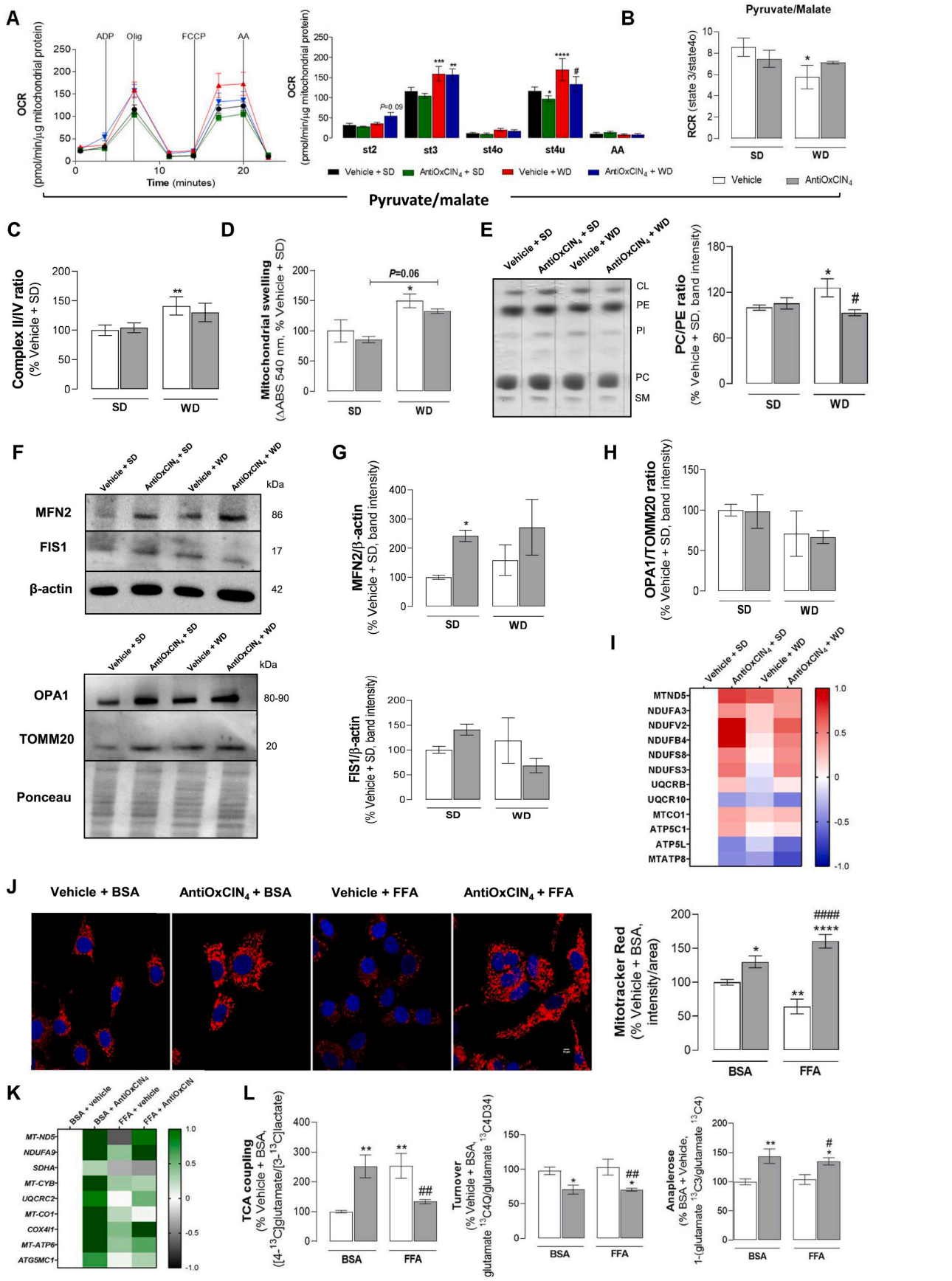


*(caption on next page)*

**Fig. 4. Effects of AntiOxCIN$_4$ on mitochondrial function of a WD-fed mice with NAFL phenotype and FFAs-treated human HepG2 cells.** (A) Oxygen consumption rate (OCR) of Complex I-linked respiration (pyruvate/malate, 10 mM/5 mM) in isolated liver mitochondria from WD-fed mice in the absence/presence of AntiOxCIN$_4$ (2.5 mg/day/animal). Adenosine di-phosphate (ADP) (4 mM), oligomycin (olig) (2 μg/μL), carbonyl cyanide-p-trifluoromethoxyphenylhydrazone (FCCP) (4 μM) and antimycin A (AA) (2 μM) were sequentially added to modulate mitochondrial function as described in SI. (B) Respiratory control ratio (RCR) (state 3/state 4) of pyruvate/malate-energized isolated liver mitochondria of WD-fed mice in the absence/presence of AntiOxCIN$_4$ (2.5 mg/day/animal). (C) Mitochondrial swelling after induction of the mitochondrial permeability transition pore opening by tBHP and $CaCl_2$in succinate-energized isolated liver mitochondria from WD-fed mice in the absence/presence of AntiOxCIN$_4$ (2.5 mg/day/animal). (D) Phosphatidylcholine/phosphatidylethanolamine (PC/PE) ratio quantification and representative image of phospholipid quantification in isolated liver mitochondria from WD-fed mice in the absence/presence of AntiOxCIN$_4$ (2.5 mg/day/animal) using TLC. The quantification of cardiolipin (CL), phosphatidylethanolamine (PE), phosphatidylcholine (PC), phosphatidylinositol (PI) and sphingomyelin (SM) are presented in Fig. S3. (E) MS-proteomic analysis of mitochondrial OXPHOS complexes subunits protein levels in liver homogenates from WD-fed mice in the absence/presence of AntiOxCIN$_4$ (2.5 mg/day/animal). Blue color represents a decrease, while red color represents an increase of protein levels. (F) Typical Western blot result of whole-liver homogenates depicting the cytosolic protein levels of Fis1, Mfn2, Opa-1 and TOMM20 from WD-fed mice in the absence/presence of AntiOxCIN$_4$ (2.5 mg/day/animal). These blots were inverted and contrast-optimized for visualization purposes. Quantification of the bands was performed using the original blots. Quantification of protein levels in multiple experiments were normalized to β-actin (cytosolic marker) levels. (G) Mfn2 and Fis1-protein levels and (H) Opa-1/TOMM20 ratio. (I) Mitochondrial electron transport chain complex activity (II/IV ratio) in isolated liver mitochondria of WD-fed mice in the absence/presence of AntiOxCIN$_4$ (2.5 mg/day/animal). (J) Typical background-corrected images of HepG2 cells stained with the fluorescent cation MitoTracker Red FM (red) and Hoechst 33342 (blue) and treated with vehicle (BSA) or FFAs (24 h, 250 μM) in the absence/presence of AntiOxCIN$_4$ (48 h, 100 μM). The MitoTracker Red FM and Hoechst 33342 fluorescence intensity was color-coded to red and blue, respectively. Average mitochondrial MitoTracker Red fluorescence intensity was calculated from four imagens in three independent experiments. (K) mRNA transcript levels of mitochondrial OXPHOS complexes subunits genes (*MT-ND5, NDUFA9, SDHA, MT-CYB, UQCRC2, MT-CO1, COX4I1, ATP6* and *ATG5G1*) in cells treated with vehicle (BSA) or FFA (24 h, 250 μM) in the absence/presence of AntiOxCIN$_4$ (48 h, 100 μM). (L) TCA coupling - [1,6–$^{13}$C2]glucose consumption coupled to TCA cycle ([4–$^{13}$C]glutamate/[3–$^{13}$C]lactate); TCA cycle turnover (glutamate $^{13}$C4Q/glutamate $^{13}$C4D34); Anaplerosis [1-(glutamate $^{13}$C3/glutamate $^{13}$C4)]. Data are expressed as the mean ± SEM (N = 5 per cage for the *in vivo* study and N = 4 for the HepG2 studies) and the results were normalized to the control condition (set as 100%). Statistically significant compared using two-way ANOVA followed by Fisher's LSD test for multiple comparisons (*P < 0.05, **P < 0.01, ***P < 0.0005, ****P < 0.0001 vs SD or Vehicle + BSA); ($^{\#}$P < 0.05, $^{\#\#}$P < 0.01, $^{\#\#\#\#}$P < 0.0001 vs WD or Vehicle + FFAs).

(Vehicle + WD) showed decreased levels of sphingomyelin (62%) and phosphatidylethanolamine (PE) (77%), with the latter contributing to an increase of phosphatidylcholine (PC)/PE ratio (126%) (Figs. 4E and S3E). Importantly, AntiOxCIN$_4$ supplementation decreased cardiolipin levels (85%) when compared with Vehicle + WD (110%), while maintaining PC/PE ratio to levels similar to the SD-fed groups (93%) (Figs. 4E and S3E). AntiOxCIN$_4$ *per se* (SD group) did not affect mitochondrial phospholipid levels (Figs. 4E and S3E).

**AntiOxCIN$_4$ upregulated mitochondrial OXPHOS subunits and MFN2, while decreasing FIS1 protein levels in the livers of WD-fed mice with NAFL phenotype.** As mitochondrial phospholipid composition, notably PC/PE ratio, has been associated with multiple key mitochondrial functions, we next analysed the levels of several proteins involved in mitochondrial fusion and fission processes by Western Blotting (Fig. 4F). AntiOxCIN$_4$ *per se* (SD group) increased MNF2, FIS1 (Fig. 4G), OPA1 and TOMM20 protein levels (Figs. S3F and S3G). The vehicle + WD group showed no alterations in MNF2, FIS1 (Fig. 4G) and OPA1 (Fig. S3G), although a non-statistically significant increase in TOMM20 protein levels was observed (Fig. S3F). Interestingly, AntiOxCIN$_4$ supplementation in WD-fed mice further increased MFN2 (Fig. 4G) but had no effects on TOMM20 and OPA1 (Figs. S3F and S3G) protein levels. On the other hand, a non-statistically significant decrease in FIS1 protein levels was observed (Fig. 4G). Consequently, we evaluated the OPA1/TOMM20 ratio, an indicator for cristae density/ETC packing [19–21]. AntiOxCIN$_4$ *per se* (SD or WD group) had no significant effect on OPA1/TOMM20 ratio (Fig. 4H). On the other hand, the vehicle + WD group showed a non-statistically significant decrease in OPA1/-TOMM20 ratio (Fig. 4H). Interestingly, mitochondrial fusion and fission-related protein expression levels in both AntiOxCIN$_4$-treated groups (SD or WD) was correlated with a higher protein expression of OXPHOS complexes subunits, mainly at the Complex I level (MTND5, NDUFA3, NDUFV2, NDUFB4, NDUFS8, NDUFS3) (Fig. 4I). These findings suggest that AntiOxCIN$_4$ modulates mitochondrial metabolism by increasing protein levels of OXPHOS complexes subunits in the liver of WD-fed mice.

**AntiOxCIN$_4$ improved mitochondrial morphology and function of FFAs-treated human HepG2 cells.** Next, human HepG2 cells labelled with the fluorescent cation Mitotracker Red were used to evaluate the effects of AntiOxCIN$_4$ in ΔΨm of cells exposed to supra-physiologic FFAs. FFA-treated cells showed a decreased ΔΨm (65%), but the pre-incubation with AntiOxCIN$_4$ (48 h, 100 μM) not only prevented FFA-associated alterations but increased ΔΨm (160%) when compared to control cells (Fig. 4J). AntiOxCIN$_4$ induced a ΔΨm hyperpolarization (130%) in BSA-treated HepG2 cells (Fig. 4J). The cellular consequences of AntiOxCIN$_4$ and/or FFAs treatments on gene expression of mitochondrial OXPHOS-related genes were also determined. The mRNA transcripts levels were significantly increased in cells pre-treated with AntiOxCIN$_4$ (Fig. 4K). Cells treated with FFAs (24 h, 250 μM) showed decreased mRNA levels of the mitochondrial DNA-encoded NADH dehydrogenase subunit 5 of respiratory complex I gene (*MT-ND5*, 64%) and the nuclear DNA-encoded succinate dehydrogenase subunit A of respiratory complex II gene (*SDHA*, 32%) (Fig. 4K). Pre-incubation with AntiOxCIN$_4$ prevented FFAs-induced *MT-ND5 gene* mRNA depletion. However, no differences were observed in the mRNA level of *SDHA* gene (Fig. 4K). AntiOxCIN$_4$ also increased mRNA levels of other mitochondrial OXPHOS subunits genes (e.g. *NDUFA9*, *UQCRC2*, *COX4l1*, *ATP6* and *ATG5G1*) in the FFAs treated cells (Fig. 4K).

**AntiOxCIN$_4$ increased tricarboxylic acid cycle (TCA) coupling and anaplerotic processes while decreasing the TCA turnover in human FFAs-treated HepG2 cells.** To determine the AntiOxCIN$_4$ effect on TCA cycle rates, we used $^{13}$C NMR isotopomer analysis for monitoring TCA cycle intermediates. AntiOxCIN$_4$-treated human HepG2 cells in the presence of FFAs/BSA and [1,6–$^{13}$C2]glucose will generate [3–$^{13}$C]pyruvate, which can either produce[3–$^{13}$C]lactate by lactate dehydrogenase or [4$^{-13}$C]glutamate through the TCA cycle. Briefly, TCA coupling was measured by the ratio between the amount of labelling on glutamate C4 isotopomers and [U–$^{13}$C]lactate. We observed that TCA coupling is increased in AntiOxCIN$_4$ + BSA-treated human HepG2 cells (252%) (Figure 4L). Moreover, FFAs treatment also increased TCA coupling (254%), being this effect counteracted when HepG2 cells were pre-incubated with AntiOxCIN$_4$ (by 121%) (Figure 4L). TCA turnover, a ratio between [3,4,5–$^{13}$C3]glutamate and [4,5–$^{13}$C2]glutamate, was decreased in both AntiOxCIN$_4$ regimens (70% in both cases), while no alteration was observed in FFAs treatment (Figure 4L). Anaplerosis, a process responsible for replenishing TCA cycle intermediates, showed a higher ratio in AntiOxCIN$_4$-treated human HepG2 cells (143% in BSA and 135% in FFA conditions) (Figure 4L), while FFAs exposure, by itself, did not alter this process. The results suggest that AntiOxCIN$_4$ causes a higher pyruvate oxidation rate by the TCA cycle.

**AntiOxCIN$_4$ increased levels of gluconeogenic-related proteins in the liver of WD-fed mice with NAFL phenotype.** Anaplerosis is catalyzed in the liver by the combined action of mitochondrial pyruvate

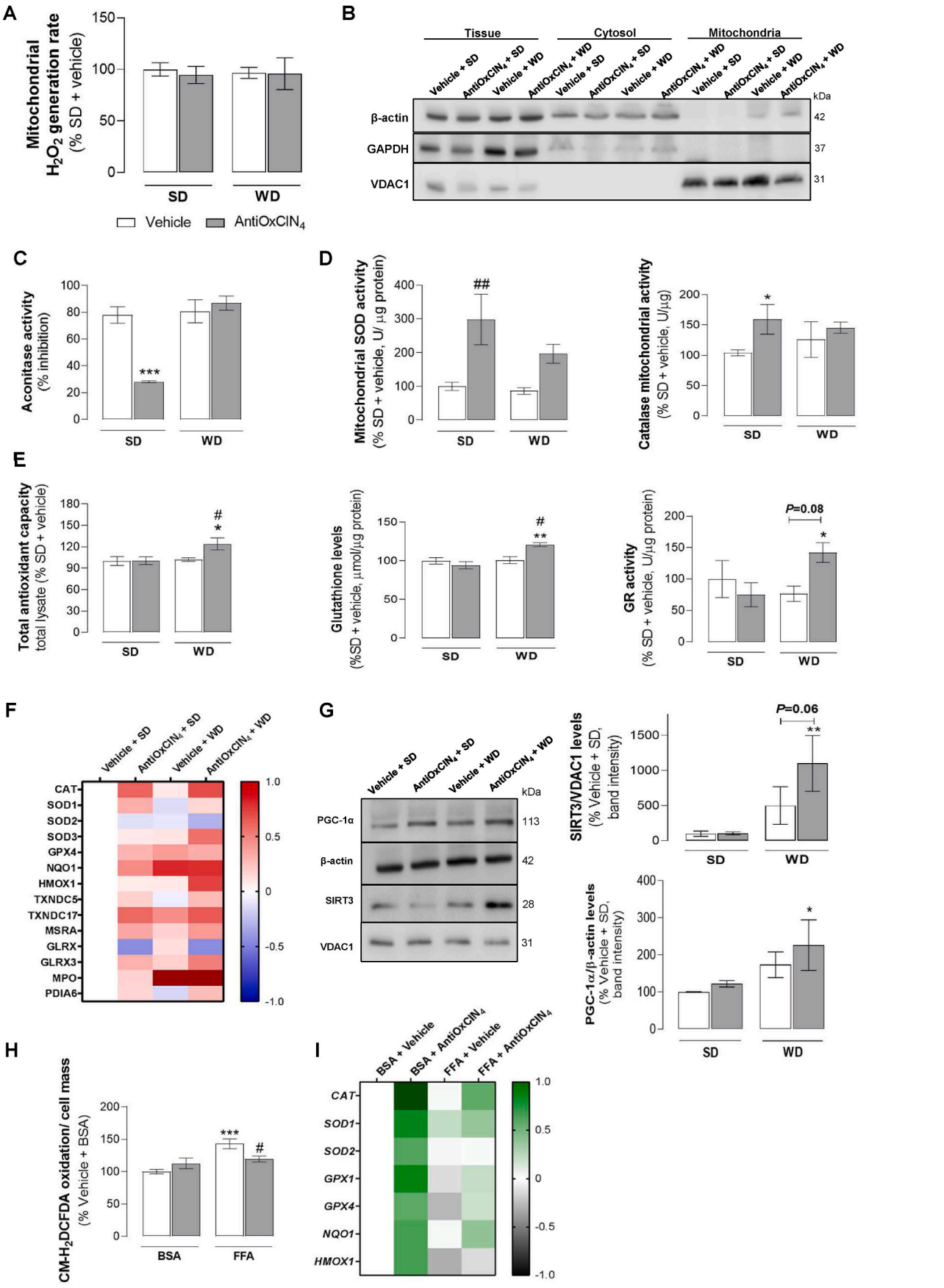


*(caption on next page)*

**Fig. 5. Effects of AntiOxCIN$_4$ on oxidative stress hallmarks and anti-oxidant defenses of a WD-fed mice with NAFL phenotype and FFAs-treated human HepG2 cells.** (A) $H_2O_2$ production rate in isolated liver mitochondria from WD-fed mice in the absence/presence of AntiOxCIN$_4$ (2.5 mg/day/animal). (B) Typical Western blot results showing the purity of cytosolic and mitochondrial fractions by using β-actin, GAPDH and VDAC1 levels. (C) Aconitase activity inhibition, superoxide dismutases (SODs) and catalase activities in isolated liver mitochondrial fraction from WD-fed mice in the absence/presence of AntiOxCIN$_4$ (2.5 mg/day/animal). (D) Total anti-oxidant capacity, glutathione reductase (GR) activity, and glutathione (GSH) levels in whole liver homogenate from WD-fed mice in the absence/presence of AntiOxCIN$_4$ (2.5 mg/day/animal). (E) MS-proteomic analysis of hepatic antioxidant-related enzymes levels in WD-fed mice in the absence/presence of AntiOxCIN$_4$ (2.5 mg/day/animal). The blue color represents a decrease, while the red color represents an increase in protein levels. (F) Typical Western blot result of whole-liver homogenates depicting the cytosolic protein levels of PGC-1α and mitochondrial protein levels of SIRT3 from WD-fed mice in the absence/presence of AntiOxCIN$_4$ (2.5 mg/day/animal). These blots were inverted and contrast-optimized for visualization purposes. Quantification of the bands was performed using the original blots. Quantification of protein levels in multiple experiments were normalized to β-actin (cytosol) or VDAC (mitochondria) levels. (G) Cellular reactive oxygen species (ROS) on HepG2 cells treated with vehicle (BSA) or FFA (24 h, 250 μM) in the absence/presence of AntiOxCIN$_4$ (48 h, 100 μM). (H) mRNA transcript levels of antioxidant-related genes (*CAT, SOD1, SOD2, GPX1, GPX4, NQO1 and HMOX1)* in cells treated with vehicle (BSA) or FFA (24 h, 250 μM) in the absence/presence of AntiOxCIN$_4$ (48 h, 100 μM) (right). The grey color represents a decrease, while the green color represents an increase of gene expression levels. Data are expressed as the mean ± SEM (N = 5 per cage for the *in vivo* study and N = 4 for the HepG2 studies) and the results were normalized to the control condition (set as 100%). Statistically significant compared using two-way ANOVA followed by Fisher's LSD test for multiple comparisons (*P < 0.05, **P < 0.01, ***P < 0.0005 vs SD or Vehicle + BSA); ($^{\#}$P < 0.05, $^{\#\#}$P < 0.01 vs WD or Vehicle + FFAs).

carboxylase (PCX) and phosphoenolpyruvate carboxykinase (PCK2), the two first enzymes of the gluconeogenic pathway [22]. In Vehicle + WD mice, PCK2 protein was diminished, while AntiOxCIN$_4$ supplementation increased both PCX and PCK2 levels (Fig. S3H). Moreover, other gluconeogenic enzymes such as phosphoglycerate kinase 2 (PGK2) and glucose-6-phosphatase (G6PC) were increased in AntiOxCIN$_4$ + WD group (Fig. S3H). AntiOxCIN$_4$ *per se* also increased PCX, G6PC and PGK2 protein levels in SD-fed mice (Fig. S3H).

**AntiOxCIN$_4$ stimulated endogenous anti-oxidant defenses in the liver of WD-fed mice with NAFL phenotype**. To understand the contribution of hepatic oxidative stress in WD-fed mice with NAFL phenotype, we next evaluated the redox status of steatotic livers. In our study, no alterations in hepatic mitochondrial $H_2O_2$ levels were observed in mice from Vehicle + WD and AntiOxCIN$_4$ + WD (Fig. 5A). As we previously described AntiOxCIN$_4$ as a redox modulator, we decided to investigate whether AntiOxCIN$_4$ impacted the mitochondrial and/or cytosolic enzymatic anti-oxidant defenses system. Consequently, mitochondria and cytosol subcellular fractions from SD- and WD-fed mice were prepared in the presence or absence of AntiOxCIN$_4$ (Fig. 5B). Aconitase is a mitochondrial enzyme whose activity is compromised with increased mitochondrial oxidative stress. Our study demonstrated that AntiOxCIN$_4$ prevented the hepatic de-activation of aconitase in SD-fed mice (Figs. 5C and S3I). In accordance, the major anti-oxidant enzymes such as superoxide dismutase (SOD) (299%) and catalase (159%) activities were increased in hepatic mitochondria from AntiOxCIN$_4$ + SD mice (Fig. 5D).

In total mice liver homogenates, anti-oxidant capacity was increased in the AntiOxCIN$_4$ + WD group (Fig. 5E). Similarly, an increase of both reduced glutathione (GSH) levels (by 27%) and glutathione reductase (GR) activity (by 67%) were observed in the AntiOxCIN$_4$ + WD group, when compared to Vehicle +SD group (Fig. 5E). Moreover, we also detected increased protein levels of several anti-oxidant defense enzymes (CAT, SOD1, TXNDC5, MSRA, GLRX3) in AntiOxCIN$_4$ + WD (Fig. 5F).

**AntiOxCIN$_4$ increased PGC-1α and mitochondrial SIRT3 protein levels in the liver of WD-fed mice with NAFL phenotype**. As PGC-1α-SIRT3 pathway drives glutamine metabolism and reduces oxidative stress, we next analysed the protein levels of mitochondrial SIRT3 and peroxisome proliferator-activated receptor-gamma coactivator (PGC-1α) by Western Blotting (Fig. 5G). Vehicle + WD group showed a non-statistically significant increase in SIRT3 (5-fold) and PGC-1α (173%) protein levels (Fig. 5G). Interestingly, AntiOxCIN$_4$ supplementation in WD-fed mice further amplified that effect by 603% in SIRT3 and 53% in PGC-1α (Fig. 5G). Notwithstanding, AntiOxCIN$_4$ *per se* (SD group) did not affect SIRT3 or PGC-1α protein levels (Fig. 5G).

**AntiOxCIN$_4$ decreased FFAs-induced ROS in human HepG2 cells by rising endogenous anti-oxidant defense gene expression**. The effect of AntiOxCIN$_4$ on the redox status and anti-oxidant defense system of human hepatoma cells (HepG2) incubated with supraphysiological concentrations of FFA was also evaluated. Oxidation of the redox-sensitive dye CM-$H_2$DCFDA in human HepG2 cells was augmented in Vehicle + FFA (24 h, 250 μM) (143%) (Fig. 5H), an effect that was remarkably prevented in AntiOxCIN$_4$ + FFA (48 h, 100 μM) (by 24%) (Fig. 5H). Although AntiOxCIN$_4$ *per se* (AntiOxCIN$_4$ + BSA) increased mRNA transcripts of *CAT, SOD1, SOD2, GPX1, GPX4, NQO1,* and *HMOX1* genes, in the presence of FFA (AntiOxCIN$_4$ + FFA) only mRNA transcripts of *CAT, SOD1, GPX1, GPX4* and *NQO1* genes were augmented by AntiOxCIN$_4$ treatment (Fig. 5I).

**AntiOxCIN$_4$ did not alter the AKT/mTOR/S6K1/4E-BP1 pathway in the liver of WD-fed mice with a NAFL phenotype**. To understand the impact of AntiOxCIN$_4$ on PI3K-AKT-mTOR pathway, which can impact disease progression, we evaluated the content of several proteins through Western Blotting analysis (Fig. S4A). In the Vehicle + WD group, we observed increased phosphorylation at Ser473 (248%) of the protein kinase B complex (AKT) and a non-significant increase in mTOR phosphorylation at Ser2448 (143%) (Fig. S4B). The decrease of AMPKα phosphorylation (Thr172) (51%) can reinforce the activation of AKT/mTOR pathway with subsequent phosphorylation of downstream proteins responsible for the induction of protein synthesis: p-p70 S6K1 (Thr389) (262%) and p-eIF4E-binding protein 1(4E-BP1) (Thr45) (392%) (Figs. S4A and B). Similar results were observed in AntiOxCIN$_4$ + WD mice, with increased levels of p-AKT (320%), p-mTOR (192%), p-p70 S6K1 (300%) and p-4EBP1 (601%), and decreased levels of p-AMPKα (33%) (Figs. S4A and B). AntiOxCIN$_4$ *per se* had no significant effect in AKT/mTOR axis and related downstream pathways in SD-fed mice (Figs. S4A and B).

**AntiOxCIN$_4$ prevented autophagy impairment in the liver of WD-fed mice with a NAFL phenotype**. Decreased autophagic flux, resulting from altered AKT/mTOR axis regulation, has been described to contribute to NAFLD pathophysiology and disease progression [23]. Several autophagic markers were evaluated to determine AntiOxCIN$_4$ ability to counteract WD-induced autophagy impairment (Fig. 6A). Vehicle + WD treatment increased LC3II/LC3I ratio (225%) and p62 (267%), and decreased Beclin1 protein levels (54%), thereby indicating autophagosome accumulation (Fig. 6B). AntiOxCIN$_4$ supplementation in WD-fed mice prevented autophagosome accumulation as measured by the increase in LC3II/LC3I ratio (by 55%) and the maintenance of p62 (112%) and Becliny1 (92%) protein levels in similar levels to the SD groups (Fig. 6B). AntiOxCIN$_4$ *per se* had no significant effect in autophagic markers in SD-fed mice (Fig. 6B).

Mitophagy constitutes an essential cellular process for mitochondrial quality control by eliminating dysfunctional mitochondria and maintaining mitochondrial homeostasis [24]. WD-fed mice showed a non-statistically significant increase of Parkin (176%), while no alterations were observed in Pink1 (93%) protein levels (Fig. 6B). AntiOxCIN$_4$ increased Parkin (219%) and Pink1 (130%) protein levels in SD-fed mice, but its supplementation in WD-fed mice only induced an upward trend in Parkin levels (by 126%) (Fig. 6B). In the Vehicle + WD

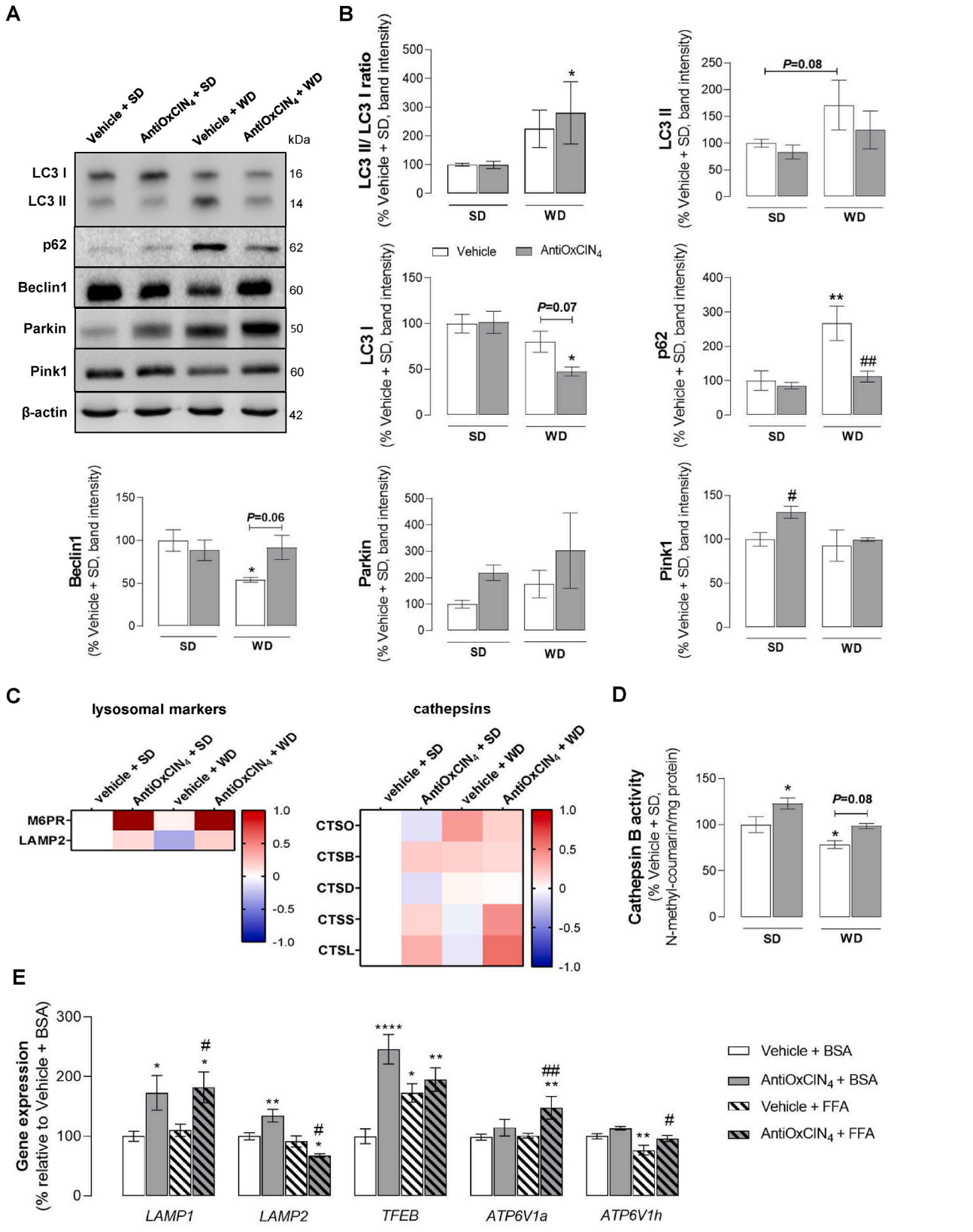


*(caption on next page)*

**Fig. 6. Effects of AntiOxCIN$_4$ on auto(mito)phagy markers in WD-fed mice with NAFL phenotype and FFAs-treated human HepG2 cells.** (A) Typical Western blot result of whole-liver homogenates depicting the protein levels of LC3BI, LC3BII, p62, Beclin1, Parkin, Pink1 and β-actin (cytosolic marker) in liver homogenates from WD-fed mice in the absence/presence of AntiOxCIN$_4$ (2.5 mg/day/animal). (B) Protein expression levels of several autophagic and/or mitophagic markers from WD-fed mice in the absence/presence of AntiOxCIN$_4$ (2.5 mg/day/animal). These blots were inverted and contrast-optimized for visualization purposes. Quantification of the bands was performed using the original blots. Quantification of proteins described above in multiple experiments was normalized to β-actin levels. Data are expressed as mean ± SEM. (C) MS-proteomic analysis of hepatic lysosomal-associated markers and cathepsins-related proteins in WD-fed mice in the absence/presence of AntiOxCIN$_4$ (2.5 mg/day/animal). The blue color represents a decrease, while the red color represents an increase in protein levels. (D) Cathepsin B activity in the whole liver homogenate from WD-fed mice in the absence/presence of AntiOxCIN$_4$ (2.5 mg/day/animal). (E) mRNA transcript levels of autophagy-related genes (*LAMP1, LAMP2, TFEB, ATP6V1a, ATP6V1H, ATP6V0e1*) in cells treated with vehicle (BSA) or FFA (24 h, 250 μM) in the absence/presence of AntiOxCIN$_4$ (48 h, 100 μM). Data are expressed as the mean ± SEM (N = 5 per cage for the *in vivo* study and N = 4 for the HepG2 studies) and the results were normalized to the control condition (set as = 100%). Statistically significant compared using two-way ANOVA followed by Fisher's LSD test for multiple comparisons (*P < 0.05, **P < 0.01, ****P < 0.0001 vs SD or Vehicle + BSA); ($^{\#}$P < 0.05, $^{\#\#}$P < 0.01 vs WD or Vehicle + FFAs).

group, a decreased autophagic flux was correlated with a reduction of the associated lysosomal membrane protein 2 (LAMP2) protein level (Fig. 6C) and cathepsin B activity (78%) (Fig. 6D) Interestingly, AntiOxCIN$_4$ supplementation prevented a WD-induced decrease in LAMP2 and increased the levels of M6PR (Fig. 6C), a receptor responsible for the binding and transport of acid hydrolases from Golgi apparatus to the lysosomes. These findings are supported by the higher protein levels of lysosomal hydrolases such as CTSS and CTSL, and higher cathepsin B activity (increased by 20%) observed in WD + AntiOxCIN$_4$ mice group (Fig. 6C and D). AntiOxCIN$_4$ also increased cathepsin B activity in the SD-fed group (122%) (Fig. 6D).

**AntiOxCIN$_4$ upregulated gene expression of lysosomal markers in FFAs-treated human HepG2 cells.** Next, HepG2 exposed to supraphysiological concentrations of FFA were used to evaluate lysosomal markers in FFA-treated cells in the presence or absence of AntiOxCIN$_4$ (48 h, 100 μM). FFAs-treated cells exhibited increased mRNA levels of *TFEB* gene (172%) (Fig. 6E). However, no alterations were observed in mRNA levels of lysosomal associated membrane proteins encoding genes such as *LAMP1*, *LAMP2*, *ATP6V1a* and *ATP6V0e1* (Fig. 6E). FFAs regimen decreased mRNA levels of *ATP6V1h* gene (76%) (Fig. 6E). Outstandingly, AntiOxCIN$_4$-treated cells in the presence of FFAs (24 h, 250 μM) showed an increase in mRNA levels of *TFEB* (by 25%), *LAMP1* (by 72%), *ATP6V1a* (by 47%) and *ATP6V1h* genes (by 20%), when compared to FFAs - vehicle cells (Fig. 6E). Pre-incubation with AntiOxCIN$_4$ (48 h, 100 μM) also led to increased mRNA levels of *TFEB* (245%), *LAMP1* (172%) and *LAMP2* (134%) genes in BSA-treated cells (Fig. 6E).

## 4. Discussion

Non-alcoholic fatty liver disease (NAFLD) has become a worldwide public health concern as metabolic syndrome-associated disorders rise. Although the cellular mechanisms behind NAFLD pathogenesis are still controversial, mitochondrial dysfunction is described as a key player in disease progression. Consequently, a substantial effort to develop more efficient pharmacologic strategies targeting mitochondria is underway for the prevention/treatment of NAFLD. Recently, we described that the mitochondria-targeted anti-oxidant AntiOxCIN$_4$ improved mitochondrial function by upregulating anti-oxidant defense systems and cellular quality control mechanisms (mitophagy/autophagy) [15]. Activation of endogenous ROS-protective pathways, such as the Nrf2/Keap1 pathway by AntiOxCIN$_4$ [15] can explain the cytoprotective effects and the beneficial impact on mitochondrial function in different cell lines (HepG2, SH-SY5Y or PHSF) towards a wide range of stressor inducing agents (iron, $H_2O_2$ or 6-hydroxydopamine (6-OHDA)) [13,16,25,26] Despite the data obtained, AntiOxCIN$_4$ *in vivo* effects on cellular and mitochondrial energy metabolism were not studied.

As mitochondrial function, namely ATP generation, are particularly affected in NAFL/NAFLD patients [27] and in animal models due to FFAs overload and subsequent higher FAO demand [28], we hypothesize that AntiOxCIN$_4$ daily supplementation can be beneficial to C57BL/6 mice fed with a high-fat (30%) plus high-sucrose (30%) diet for 16 weeks [29], which mimics WD (high-fat, high-sugar) habits. WD feeding induced abnormal body weight gain and visceral adiposity, with increased circulating plasma AST and ALT levels suggesting hepatocyte damage. The absence of evident inflammatory markers and signs of fibrosis confirmed the development of NAFL, an early NAFLD stage. Nevertheless, we observed that WD feeding caused TG accumulation, which presented higher content in oleate, and reduced amounts of linoleate and ω-3 FAs. AntiOxCIN$_4$ supplementation prevented body weight gain in WD-fed mice, reducing liver weight and fat deposition, and improved ALT and AST levels. The reduction of hepatic steatosis was correlated with a lower TG content, being the LD number and size decreased in our *in vitro* model. The effects of AntiOxCIN$_4$ appear not to be correlated with significant alterations in proteins involved in FFAs influx and the DNL pathway. Nevertheless, we found higher protein levels of elongases ELOVL1 and 5. Notably, AntiOxCIN$_4$ supplementation prevented the above-described alterations, mainly regarding ω-3 FAs. In fact, higher ELOVL5 activity and ω-3 FAs levels could ameliorate the above-described hepatic parameters. This is in line with studies showing that increased TG catabolism and reducing ER stress in obese mice [30] and, ω-3 PUFA supplementation had beneficial effects on decreasing blood TG levels [31], and PPARs activation, which in turn increased hepatic FAO [32], and autophagic degradation [33]. Fatty acid oxidation enhancement is often observed in NAFLD due to increased hepatic uptake and *de novo* lipogenesis [34]. Our NAFL mouse model showed upregulation of mitochondrial and peroxisomal FAO-related protein levels, which indicated an adaptive response to FAs overload. Increased mitochondrial and peroxisomal FAO-related protein levels were also observed in AntiOxCIN$_4$ + SD mice, supporting the hypothesis that AntiOxCIN$_4$ can restrain lipotoxicity by boosting both mitochondrial and peroxisomal FAO. FAO is often associated with increased acetylCoA pools, which can result in: a) *de novo* lipogenesis; b) TCA cycle; c) ceramides synthesis and inflammation; d) ketogenesis and e) cholesterol synthesis. In the absence of inflammatory processes, decreased TAG content and TCA turnover, fatty acids in the blood are converted to ketone bodies when insulin is low, and the fatty acid concentration is high. Fatty acyl CoA is transported into the liver mitochondria by the carnitine shuttle system. The movement of fatty acyl CoA molecules across the mitochondrial membrane involves carnitine palmityl transferase I (CPT-I) protein, which AntiOxCIN$_4$ clearly increases. Metabolic improvements in WD-fed mice supplemented with AntiOxCIN$_4$ may rely on augmented FAO that favours the clearance of lipid accumulation, thereby preventing lipotoxicity-associated injury and more advanced steatotic phenotypes [35]. In fact, several reports have been pointing out the importance of ketogenesis to improve NAFLD [36–38].

NAFLD pathophysiology is associated with altered lipid homeostasis that, together with other unbalanced processes such as increased OxS, mitochondrial dysfunction or autophagic blockage, may progress towards a more severe phenotype. Increased mtROS levels or mitochondrial-associated OxS were not observed in WD-fed mice, while supraphysiological concentrations of FFAs increased total cellular (mainly peroxisomal) ROS in human HepG2 cells. Nevertheless, AntiOxCIN$_4$ pre-treatment significantly attenuated cellular increased ROS production. Recent literature argues that peroxisomal $H_2O_2$ rather than

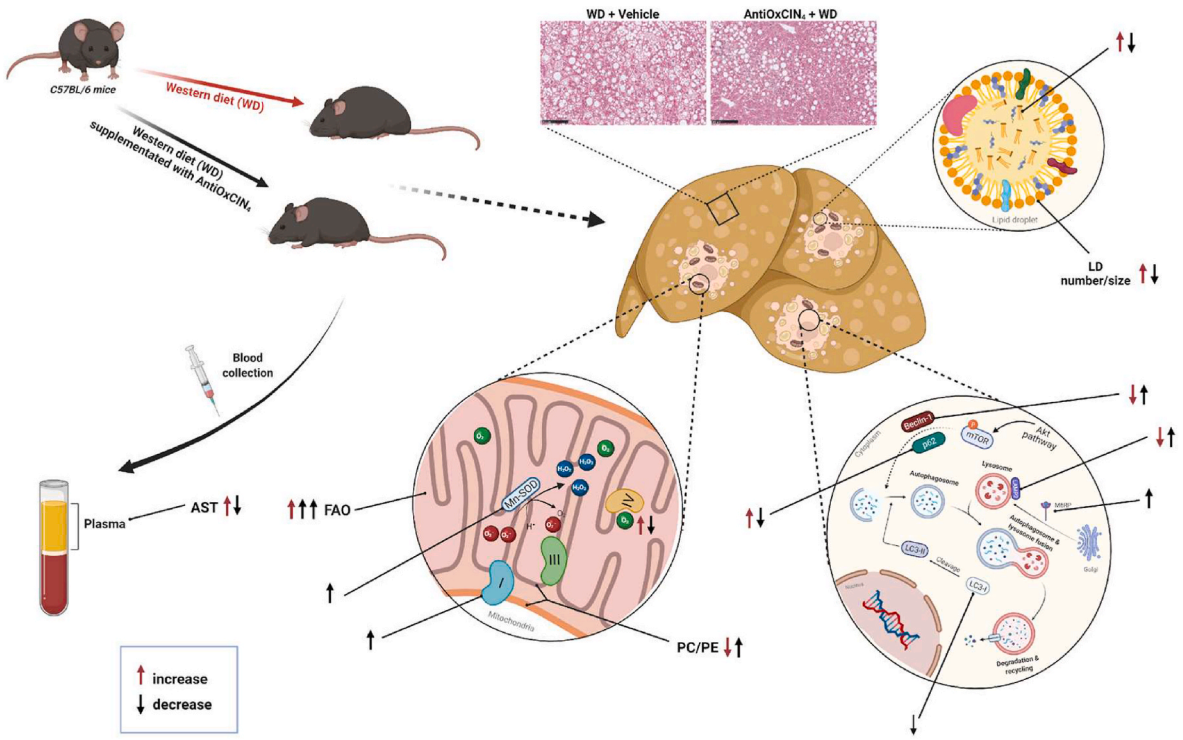


**Fig. 7. Schematic diagram summarizing the effects of mitochondriotropic anti-oxidant AntiOxCIN$_4$ supplementation in a WD-fed mice with NAFL phenotype.** AntiOxCIN$_4$ supplementation reduced body weight gain of mice fed with a Western diet (WD) for 16 weeks. AntiOxCIN$_4$ also decreased liver weight with amelioration of hepatic damage markers (aspartate aminotransferase (AST)) and decreased steatosis with a reduction in the number/size of lipid droplets. These effects were shown to be partly attributed to increased fatty acid oxidation (FAO). AntiOxCIN$_4$ supplementation promoted a mitochondrial remodeling, which resulted in increased protein levels of Complex I subunits, prevention of WD modification on phosphatidylcholine/phosphatidylethanolamine (PC/PE) levels. Additionally, an induction of endogenous anti-oxidant defense system was also observed, with higher activity of mitochondrial superoxide dismutase (SOD). Furthermore, AntiOxCIN$_4$ prevented WD-induced impairment of autophagy quality control mechanism as shown by the avoidance of p62 accumulation and the maintenance of Beclin-1 and LC3-II protein levels. Moreover, AntiOxCIN$_4$ additionally increased lysosomal proteolytic activity as shown by higher lysosome-associated membrane glycoprotein 2 (LAMP2) and mannose-6-phosphate receptor (M6PR) levels. The amelioration of whole-body mouse parameters and especially, a healthier phenotype of hepatocytes support the use of AntiOxCIN$_4$ as a great potential agent for the prevention/treatment of NAFLD (details in Discussion).

mitochondrial $H_2O_2$ contributed to ROS production in the early stages of NAFLD [39,40]. In fact, peroxisomes are also a critical organelle contributing to ROS generation through **β**-oxidation while other cellular oxidases can also generate $H_2O_2$ [41]. Even in the absence of abnormal mitochondrial $H_2O_2$, AntiOxCIN$_4$ stimulated the endogenous anti-oxidant defense system, particularly GSH, mitochondrial SOD, and peroxisomal catalase. Upregulation of the endogenous anti-oxidant defense system by AntiOxCIN$_4$ treatment can attenuate the overall OxS. Our data indicate that PGC-1α-SIRT3 axis interplay regulates these processes. SIRT3 showed to control global mitochondrial protein acetylation level, mitochondrial redox status, epigenetic regulation, and lipid homeostasis in the liver [42]. Moreover, PGC-1α, the main regulator of mitochondrial biogenesis, stimulates SIRT3 expression in a regulatory pathway that drives mtROS generation and mitochondrial biogenesis [43,44]. The effect on the PGC-1α-SIRT3 axis increased the anti-oxidant capacity of AntiOxCIN$_4$-treated animals and cells. This is in line with our previous observations that AntiOxCIN$_4$ induced an Nrf2-dependent cellular adaptative response mediated and triggered by a sustainable increase in mtROS, which led to an upregulation of the cellular anti-oxidant defense system that protected HepG2 cells against the detrimental effects subsequent oxidative stress insults [15].

WD feeding induced remodeling of the mitochondrial metabolism with altered TCA cycle fluxes, augmented electron transport chain activity and respiration and altered mitochondrial membrane composition with a decreased RCR and a higher susceptibility for mPTP-mediated membrane permeabilization. AntiOxCIN$_4$ supplementation plays a role in mitochondrial homeostasis by upregulating OXPHOS complexes subunits (mainly at complex I) gene/protein expression levels by increasing MFN2 and decreasing FIS1 protein levels but not the cristae density/ETC packing, preventing WD-induced PC/PE ratio abnormalities [45] and RCR, and slightly protecting mitochondria from mPTP opening episodes induced by $Ca^{2+}$/*t*BHP in the liver of WD-fed mice with NAFL. Moreover, we observed that FFAs-treated human HepG2 cells showed increased TCA coupling [46]. As mitochondrial TCA cycle intermediates are not stored, the pathways of anaplerosis and cataplerosis operate continuously at the same rate. AntiOxCIN$_4$-treated human HepG2 cells increased anaplerotic fluxes and β-oxidation processes, which corroborate the observation that β-oxidation and the generation of acetyl-CoA increase anaplerotic capacity [47]. Anaplerosis is also indispensable for urea cycle function and anti-oxidant defenses, by maintaining NADPH pool [48]. WD-fed mice showed a decrease in some gluconeogenic-related proteins (G6PC; PGK2), which was prevented by AntiOxCIN$_4$ supplementation. Moreover, AntiOxCIN$_4$ supplementation also increased PCX and mitochondrial isoform of PCK2 protein levels in WD-fed mice. PCX is essential not only to fuel TCA cycle but also to provide substrates for non-enzymatic anti-oxidant defense system build-up [48]. In our *in vitro* model, AntiOxCIN$_4$ decreased TCA cycle turnover, limiting citrate cataplerosis used in lipogenesis, possibly explaining the decrease in TG content in the whole liver form WD-fed mice supplemented with AntiOxCIN$_4$.

Diet-induced NAFLD is associated with AKT/mTORC signaling activation. In this pathway, the active form of mTORC1 phosphorylates S6K1, resulting in cellular translation and cell growth mediated by 4E-BP1 [49]. Our *in vivo* NAFL model showed that WD feeding upregulated the AKT/mTOR/S6K1/4E-BP1 pathway, leading to mTORC activation and blockage of autophagic flux. Remarkably, AntiOxCIN$_4$

maintains or increases normal autophagic flux. Moreover, we observed up-regulation of the Pink1-Parkin protein levels axis in SD-fed mice supplemented with AntiOxCIN$_4$. Although autophagy and mitophagy can contribute to hepatocyte adaptation due to the specific degradation of LD (lipophagy) in NAFL, quality control impairment have been linked to NASH progression [50,51]. We propose that AntiOxCIN$_4$ can overcome autophagic blockage resulting from defective lysosomal acidification [52] by improving the lysosomal number and proteolytic activity, which can counteract the accumulation of damaged mitochondria or other subcellular structures and protect hepatocytes from lipotoxicity insults in NAFLD-associated conditions. In fact, we have previously found that AntiOxCIN$_4$ pre-treatment increased lysosomal content in both fibroblasts from Parkinson's disease patients [25] and human hepatoma-derived HepG2 cells [15], as well as, AntiOxCIN$_4$-treated HepG2 cells increased lysosomes co-localized with the mitochondria [15].

In summary, our pioneering study has shown for the first time the beneficial role of AntiOxCIN$_4$ supplementation *in vivo* in the early NAFL stage. Using a WD-fed mice model, and mechanistically complementing and translating data with human hepatic HepG2 cells, we pointed out the AntiOxCIN$_4$ improves a steatotic liver phenotype. In addition to a decrease in body weight gain, AntiOxCIN$_4$ decreased hepatic steatosis by decreasing LD number/size and its composition. Importantly, these effects were correlated with increased cellular FAO activity. The mitochondriotropic anti-oxidant AntiOxCIN$_4$ improved mitochondrial function by upregulating anti-oxidant defense systems and cellular quality control mechanisms (mitophagy/autophagy), strengthening hepatic mitochondria and increasing their resistance to further oxidative damage in the later NAFLD stages. The amelioration of whole-body parameters in WD-fed mice and especially, a healthier phenotype of hepatocytes supports the use of AntiOxCIN$_4$ as a potential candidate for the prevention/treatment of NAFLD (Fig. 7).

## Author contribution

RA, ICMS, JT, YP, AC, SPP and RFS performed the experiments. AKW and SS performed the histological assessment. JJ and AD performed the lipidomic analysis. LCT and JGJ performed the NMR experiments. IV performed plasma analysis. MD analysed mass spectrometry proteomic data. FC, PS and SB synthesized the mitochondria-targeted anti-oxidant AntiOxCIN$_4$. TCO performed the principal component analysis of the data. RA, ICMS, JT, YP, MRW and PJO analysed the data. RA, ICMS, JT, MRW and PJO wrote the manuscript. All the authors revised the final version of the manuscript. JT, FB, MRW and PJO supervised the research.

## Declaration of competing interest

Paulo J. Oliveira and Fernanda Borges are cofounders of the CNC-UP spin-off company MitoTAG (Coimbra, Portugal). This spin-off had no involvement in the data collection, analysis and interpretation, manuscript writing, and the decision to submit the manuscript for publication.

## Acknowledgements

This work was funded by FEDER funds through the Operational Programme Competitiveness Factors (COMPETE) and the Foundation for Science and Technology (FCT): EXPL/BIA-BQM/1361/2021, PTDC/BIA-MOL/28607/2017, POCI-01-0145-FEDER-028607, PTDC/BTM-SAL/29297/2017, POCI-01-0145-FEDER-029297, UIDB/04539/2020, UIDP/04539/2020 and UIDP/QUI/00081/2020). Support for RA (SFRH/BD/131070/2017), AC (SFRH/BD/140817/2018), RFS (SFRH/BPD/116061/2016) and SPP (PD/BD/128254/2016) was provided by FCT, POPH and QREN. JT (2020.01560.CEECIND) and TCO (DL57/2016/CP1448/CT0016) acknowledges FCT, I.P. for the research contracts. MRW was supported by the National Science Centre, Poland (grant UMO-2018/29/B/NZ1/00589). ICMS was supported by the National Science Centre (grant UMO-2020/36/T/NZ1/00004). Additionally, I.C.M.S., J.G.J, M.R.W. and P.J.O. gratefully acknowledge the financial support for this research from the FOIE GRAS and mtFOIE GRAS projects. These projects received funding from the European Union's Horizon 2020 Research and Innovation programme under the Marie Skłodowska-Curie Grant Agreement No. 722619 (FOIE GRAS) and Grant Agreement No. 734719 (mtFOIE GRAS). We also acknowledge the DMPK team led by Professor Kevin Read from the Wellcome Centre for Anti-Infectives Research (WCAIR) at the School of Life Sciences of the University of Dundee for performing the studies of AntiOxCin4 stability in water. Fig. 7 was drawn with BioRender software.

## Appendix A. Supplementary data

Supplementary data to this article can be found online at https://doi.org/10.1016/j.redox.2022.102400.

## References

[1] M. Masarone, et al., Role of oxidative stress in pathophysiology of nonalcoholic fatty liver disease, 2018, Oxid. Med. Cell. Longev. (2018), 9547613.
[2] A.J. Sanyal, et al., Pioglitazone, vitamin E, or placebo for nonalcoholic steatohepatitis, N. Engl. J. Med. 362 (18) (2010) 1675–1685.
[3] V.J. Navarro, et al., Correction: silymarin in non-cirrhotics with non-alcoholic steatohepatitis: a randomized, double-blind, placebo controlled trial, PLoS One 14 (10) (2019), e0223915.
[4] I. Grattagliano, et al., Targeting mitochondria to oppose the progression of nonalcoholic fatty liver disease, Biochem. Pharmacol. 160 (2019) 34–45.
[5] H. Rehman, et al., The mitochondria-targeted anti-oxidant MitoQ attenuates liver fibrosis in mice, Int J Physiol Pathophysiol Pharmacol 8 (1) (2016) 14–27.
[6] B.J. Snow, et al., A double-blind, placebo-controlled study to assess the mitochondria-targeted anti-oxidant MitoQ as a disease-modifying therapy in Parkinson's disease, Mov. Disord. 25 (11) (2010) 1670–1674.
[7] E.J. Gane, et al., The mitochondria-targeted anti-oxidant mitoquinone decreases liver damage in a phase II study of hepatitis C patients, Liver Int. 30 (7) (2010) 1019–1026.
[8] S. Carotti, et al., Lipophagy impairment is associated with disease progression in NAFLD, Front. Physiol. 11 (2020) 850.
[9] H.Z. Lin, et al., Metformin reverses fatty liver disease in obese, leptin-deficient mice, Nat. Med. 6 (9) (2000) 998–1003.
[10] S.F. Wang, et al., Autophagy modulators from traditional Chinese medicine: mechanisms and therapeutic potentials for cancer and neurodegenerative diseases, J. Ethnopharmacol. 194 (2016) 861–876.
[11] H.M. Kim, et al., Caffeic acid ameliorates hepatic steatosis and reduces ER stress in high fat diet-induced obese mice by regulating autophagy, Nutrition 55–56 (2018) 63–70.
[12] S.J. Wang, et al., Bioavailability of caffeic acid in rats and its absorption properties in the Caco-2 cell model, Pharm. Biol. 52 (9) (2014) 1150–1157.
[13] J. Teixeira, et al., Mitochondria-targeted phenolic anti-oxidants induce ROS-protective pathways in primary human skin fibroblasts, Free Radic. Biol. Med. 163 (2021) 314–324.
[14] C.M. Deus, et al., Mitochondrial remodeling in human skin fibroblasts from sporadic male Parkinson's disease patients uncovers metabolic and mitochondrial bioenergetic defects, Biochim. Biophys. Acta, Mol. Basis Dis. 1866 (3) (2020), 165615.
[15] R. Amorim, et al., Mitochondriotropic anti-oxidant based on caffeic acid AntiOxCIN, Free Radic. Biol. Med. 179 (2022) 119–132.
[16] J. Teixeira, et al., Development of a mitochondriotropic antioxidant based on caffeic acid: proof of concept on cellular and mitochondrial oxidative stress models, J. Med. Chem. 60 (16) (2017) 7084–7098.
[17] K. Begriche, et al., Mitochondrial adaptations and dysfunctions in nonalcoholic fatty liver disease, Hepatology 58 (4) (2013) 1497–1507.
[18] I. Martínez-Reyes, N.S. Chandel, Mitochondrial TCA cycle metabolites control physiology and disease, Nat. Commun. 11 (1) (2020) 102.
[19] D.A. Patten, et al., OPA1-dependent cristae modulation is essential for cellular adaptation to metabolic demand, EMBO J. 33 (22) (2014) 2676–2691.
[20] H. Lee, Y. Yoon, Mitochondrial membrane dynamics-functional positioning of OPA1, Antioxidants 7 (12) (2018). Basel.
[21] S. Cogliati, et al., Mitochondrial cristae shape determines respiratory chain supercomplexes assembly and respiratory efficiency, Cell 155 (1) (2013) 160–171.
[22] N.E. Sunny, et al., Excessive hepatic mitochondrial TCA cycle and gluconeogenesis in humans with nonalcoholic fatty liver disease, Cell Metabol. 14 (6) (2011) 804–810.
[23] A. González-Rodríguez, et al., Impaired autophagic flux is associated with increased endoplasmic reticulum stress during the development of NAFLD, Cell Death Dis. 5 (2014), e1179.
[24] J.J. Lemasters, Selective mitochondrial autophagy, or mitophagy, as a targeted defense against oxidative stress, mitochondrial dysfunction, and aging, Rejuvenation Res. 8 (1) (2005) 3–5.

[25] C.M. Deus, et al., A mitochondria-targeted caffeic acid derivative reverts cellular and mitochondrial defects in human skin fibroblasts from male sporadic Parkinson's disease patients, Redox Biol. 45 (2021), 102037.
[26] S. Benfeito, et al., Fine-tuning the neuroprotective and blood-brain barrier permeability profile of multi-target agents designed to prevent progressive mitochondrial dysfunction, Eur. J. Med. Chem. 167 (2019) 525–545.
[27] C. Koliaki, et al., Adaptation of hepatic mitochondrial function in humans with non-alcoholic fatty liver is lost in steatohepatitis, Cell Metabol. 21 (5) (2015) 739–746.
[28] R.E. Patterson, et al., Lipotoxicity in steatohepatitis occurs despite an increase in tricarboxylic acid cycle activity, Am. J. Physiol. Endocrinol. Metab. 310 (7) (2016) E484–E494.
[29] I.C.M. Simoes, et al., Western diet causes obesity-induced nonalcoholic fatty liver disease development by differentially compromising the autophagic response, Antioxidants 9 (10) (2020).
[30] S. Tripathy, et al., Fatty acid elongase-5 (Elovl5) regulates hepatic triglyceride catabolism in obese C57BL/6J mice, J. Lipid Res. 55 (7) (2014) 1448–1464.
[31] H.M. Parker, et al., Omega-3 supplementation and non-alcoholic fatty liver disease: a systematic review and meta-analysis, J. Hepatol. 56 (4) (2012) 944–951.
[32] W. Lu, et al., 2016, Effects of Omega-3 Fatty Acid in Nonalcoholic Fatty Liver Disease: A Meta-Analysis, Gastroenterol Res Pract, 2016, 1459790.
[33] Y. Chen, et al., ω-3 Fatty acids reverse lipotoxity through induction of autophagy in nonalcoholic fatty liver disease, Nutrition 31 (11–12) (2015), 1423-1429.e2.
[34] D.H. Ipsen, J. Lykkesfeldt, P. Tveden-Nyborg, Molecular mechanisms of hepatic lipid accumulation in non-alcoholic fatty liver disease, Cell. Mol. Life Sci. 75 (18) (2018) 3313–3327.
[35] G. Naguib, et al., Dietary fatty acid oxidation is decreased in non-alcoholic fatty liver disease: a palmitate breath test study, Liver Int. 40 (3) (2020) 590–597.
[36] G. Patman, NAFLD: ketogenesis could be a determinant of steatohepatitis, Nat. Rev. Gastroenterol. Hepatol. 11 (12) (2014) 702.
[37] P.K. Luukkonen, et al., Effect of a ketogenic diet on hepatic steatosis and hepatic mitochondrial metabolism in nonalcoholic fatty liver disease, Proc. Natl. Acad. Sci. U. S. A. 117 (13) (2020) 7347–7354.
[38] J.A. Fletcher, et al., Impaired ketogenesis and increased acetyl-CoA oxidation promote hyperglycemia in human fatty liver, JCI Insight 5 (2019).
[39] E.M. Morris, et al., Aerobic capacity mediates susceptibility for the transition from steatosis to steatohepatitis, J. Physiol. 595 (14) (2017) 4909–4926.
[40] I.C.M. Simões, et al., The alterations of mitochondrial function during NAFLD progression-an independent effect of mitochondrial ROS production, Int. J. Mol. Sci. 22 (13) (2021).
[41] L.M. Sandalio, et al., Role of peroxisomes as a source of reactive oxygen species (ROS) signaling molecules, Subcell. Biochem. 69 (2013) 231–255.
[42] J. Zhang, et al., Mitochondrial Sirtuin 3: new emerging biological function and therapeutic target, Theranostics 10 (18) (2020) 8315–8342.
[43] E. Barroso, et al., SIRT3 Deficiency exacerbates fatty liver by attenuating the HIF1α-LIPIN 1 pathway and increasing CD36 through Nrf2, Cell Commun. Signal. 18 (1) (2020) 147.
[44] X. Kong, et al., Sirtuin 3, a new target of PGC-1alpha, plays an important role in the suppression of ROS and mitochondrial biogenesis, PLoS One 5 (7) (2010), e11707.
[45] J.N. van der Veen, et al., The critical role of phosphatidylcholine and phosphatidylethanolamine metabolism in health and disease, Biochim. Biophys. Acta Biomembr. 1859 (9 Pt B) (2017) 1558–1572.
[46] R. Amorim, et al., Exploratory data analysis of cell and mitochondrial high-fat, high-sugar toxicity on human HepG2 cells, Nutrients 13 (5) (2021).
[47] H.M. White, The role of TCA cycle anaplerosis in ketosis and fatty liver in periparturient dairy cows, Animals 5 (3) (2015) 793–802.
[48] D.A. Cappel, et al., Pyruvate-carboxylase-mediated anaplerosis promotes anti-oxidant capacity by sustaining TCA cycle and redox metabolism in liver, Cell Metabol. 29 (6) (2019), 1291-1305.e8.
[49] R.J. Dowling, et al., Dissecting the role of mTOR: lessons from mTOR inhibitors, Biochim. Biophys. Acta 1804 (3) (2010) 433–439.
[50] X. Wang, et al., Defective lysosomal clearance of autophagosomes and its clinical implications in nonalcoholic steatohepatitis, Faseb. J. 32 (1) (2018) 37–51.
[51] R. Li, S. Toan, H. Zhou, Role of mitochondrial quality control in the pathogenesis of nonalcoholic fatty liver disease, Aging (Albany NY) 12 (7) (2020) 6467–6485.
[52] Y. Inami, et al., Hepatic steatosis inhibits autophagic proteolysis via impairment of autophagosomal acidification and cathepsin expression, Biochem. Biophys. Res. Commun. 412 (4) (2011) 618–625.